IN-WHEEL MOTOR DESIGN
FOR ELECTRIC VEHICLES

By
KAZIM ÇAKIR

Submitted to the Graduate School of Engineering and Natural Sciences
in partial fulfillment of
the requirements for the degree of
Master of Science

SABANCI UNIVERSITY
Spring 2004

IN-WHEEL MOTOR DESIGN
FOR ELECTRIC VEHICLES

APPROVED BY:

Prof. Dr. ASIF ŞABANOVİÇ .....
(Dissertation Advisor)

Assistant Prof. Dr. AHMET ONAT .....

Assistant Prof. Dr. ERHAN BUDAK .....

DATE OF APPROVAL: .....

© Kazım Çakır 2004
All Rights Reserved

ABSTRACT

In this thesis an in-wheel electric motor prototype has been designed for experimental purposes. In-Wheel Motor (Hub motor) can be used in electric cars with 4 wheel independent drive configuration. Within every wheel, there can be one "Direct-Drive In-Wheel Motor" to generate the necessary torque per wheel. Unlike conventional "central drive unit" systems, torque as well as the power and speed can be supplied to each tyre independently.

The difference in this work is the design of a direct drive electric motor which is able to carry transverse loading acts on the tyre. Type of the motor is called inverted configuration or outer rotor structure in the literature, in which the rotating element is the casing of the motor.

The electric machine designed in the thesis is Switched Reluctance Machine. First a 3D solid model was created. Necessary strength analyses have been done. Simultaneously, electromagnetic FEA have been done, when it is necessary either of the designs were modified until it converged to a set of consistent dimensions for both mechanic and electromagnetic design.

Last, the results of the electromagnetic analysis were embedded into a hybrid simulation model, in order to check the coherency between the design and the analysis. The results were coherent.

ÖZET

Bu tezde yapılan deneysel amaçlı bir "tekerlek-içi motor" prototipidir. Tekerlek-içi motorlar 4 tekerlekten bağımsız çekişli elektrikli taşıtlarda kullanılır. Bu araçlarda her tekerleğin içine 'doğrudan-sürüş' yapısında birer tekerlek-içi motor yerleştirilir. Merkezi güç birimli yapıların aksine bu taşıtlarda güç, tork ve hız her bir tekerleğe kontrollü bir biçimde bağımsız olarak sağlanabilir.

Bu tezin içerdiği farklılıklardan birisi şaft eksenine dik, yani radyal, yükleri kaldırabilen doğrudan-sürüş yapısında bir elektrik motorunun tasarımıdır. Tasarlanan motor türü literatürde terslenmiş motor, ya da dış rotor tasarımı şeklinde geçmektedir.

Tasarım temel olarak 'Anahtarlamalı Reluktans Motor' tipindedir. İlk olarak mekanik tasarımın parçası olarak 3-Boyutlu katı modeller yaratılmış, ve gerekli dayanılılıkta olup olmadıkları sınanmıştır. Eş zamanlı olarak elektromanyetik tasarımın da sonlu-eleman-analizi yürütülmüş, gerektiği zaman her iki tasarımda yenilenerek sonuçta birbiriyle tutarlı boyut ve özellikler elde edilmiştir.

Son olarak elektromanyetik analizden edilen veriler melez bir simulasyon modeline girilerek tasarım ve analizin sonuçaları karşılaştırılmıştır. Sonuçlar tutarlıdır.

“for GONDOR…”

ACKNOWLEDGEMENTS

At the beginning, even though I was aware of it, I never thought I'd be this much into this concept. Professor Asif Sabanovic gave me the inspiration and the encouragement for it. He connected me to the experienced academicians from Kocaeli University, and supported me all the way. For his help, I would like to thank him from the bottom of my heart.

I also owe my thanks to Kocaeli side of the project. Professor Feriha Erfan Kuyumcu and his assistants Kadir Yılmaz, and Aytaç ccc helped me for weeks and weeks on this project. I would like to thank them for sharing their Fridays together with me on Maxwell.

My father, Hüseyin Çakır, spent his time and money on producing some of the parts for the motor. Thank you.

Special thanks to Feriha Sertçelik Birol from Arçelik R&D for supplying me the silicon steel rolls for free and helping me on the concept.

Finally, I would like to thank my friends; mechatronics assistants and LFI guys for making life enjoyable to me whenever I was down.

TABLE OF CONTENTS

LIST OF TABLES

LIST OF FIGURES

TABLE OF SYMBOLS

A_s	:	Specific loading (A-turns/m)
A_v	:	Vehicle's frontal projection area (m)
B	:	Flux density (Weber/m^2 = Tesla)
b_{sr}	:	Stator yoke thickness (back-iron)
b_{sy}	:	Rotor yoke thickness (back-iron)
C_d	:	Air-drag coefficient
Error! Objects cannot be created from editing field codes.	:	Bore diameter (mm)
D_o	:	Rotor outer diameter (mm)
D_s	:	Shaft diameter (mm)
D_{wire}	:	Magnet-wire diameter (m)
i	:	Current (A)
I_p	:	Peak current (A)
I_{RMS}	:	RMS current (A)
F	:	Force (N)
F_{air}	:	Air-drag (N)
F_{N_tyre}	:	Normal force acting on a tyre (N)
F_{roll}	:	Friction force due to the rolling (N)
H	:	Flux intensity (A/m)
h_{cs1}	:	Height of winding clearance from the top of the pole (m)

h_{cs2}	:	Height of winding clearance from the bottom of the pole (m)
h_r	:	Rotor pole height (m)
h_s	:	Stator pole height (m)
k_d	:	Duty ratio
k_e	:	Efficiency
L	:	Inductance (H)
Error! Objects cannot be created from editing field codes.	:	Air-gap thickness (mm)
L_s	:	Stack length (m)
L_{aa}	:	Self inductance (H)
L_{ab}	:	Mutual inductance between phase a and b (H)
n	:	Safety factor
P_d	:	Power developed (W)
P_r	:	Number of rotor poles
P_s	:	Number of stator poles
R	:	Resistance (Ω)
R_s	:	Phase resistance (Ω)
R_{wire_m}	:	Magnet wire resistance per meter (Ω/m)
T	:	Torque (Nm)
T_e	:	Electromagnetic torque (Nm)
T_f	:	Fall time (s)
T_{ph}	:	Number of coil turns per phase
v	:	Vehicle speed (m/s)
W_c	:	Co-energy (joules)
w_{coil}	:	Width of the coil (m)
w_{sp}	:	Stator pole width (m)

λ	:	Flux-linkage (V/s)
ϕ	:	Flux (weber)
μ_r	:	Rolling friction coefficient
τ	:	Shear stress (N/m^2)
σ_y	:	Yield stress (N/m^2)
ω_n	:	Rotor speed (rad/s)

TABLE OF ABBREVIATIONS

ABS	Anti Blockage System
EV	Electric Vehicle
FEA	Finite Element Analysis
SRM	Switched Reluctance Motor
VRM	Variable Reluctance Motor
ZEV	Zero Emission Vehicle

IN-WHEEL MOTOR DESIGN
FOR ELECTRIC VEHICLES

By
KAZIM ÇAKIR

Submitted to the Graduate School of Engineering and Natural Sciences
in partial fulfillment of
the requirements for the degree of
Master of Science

SABANCI UNIVERSITY
Spring 2004

IN-WHEEL MOTOR DESIGN
FOR ELECTRIC VEHICLES

APPROVED BY:

Prof. Dr. ASIF ŞABANOVİÇ .....
(Dissertation Advisor)

Assistant Prof. Dr. AHMET ONAT .....

Assistant Prof. Dr. ERHAN BUDAK .....

DATE OF APPROVAL: .....

© Kazım Çakır 2004
All Rights Reserved

ABSTRACT

In this thesis an in-wheel electric motor prototype has been designed for experimental purposes. In-Wheel Motor (Hub motor) can be used in electric cars with 4 wheel independent drive configuration. Within every wheel, there can be one "Direct-Drive In-Wheel Motor" to generate the necessary torque per wheel. Unlike conventional "central drive unit" systems, torque as well as the power and speed can be supplied to each tyre independently.

The difference in this work is the design of a direct drive electric motor which is able to carry transverse loading acts on the tyre. Type of the motor is called inverted configuration or outer rotor structure in the literature, in which the rotating element is the casing of the motor.

The electric machine designed in the thesis is Switched Reluctance Machine. First a 3D solid model was created. Necessary strength analyses have been done. Simultaneously, electromagnetic FEA have been done, when it is necessary either of the designs were modified until it converged to a set of consistent dimensions for both mechanic and electromagnetic design.

Last, the results of the electromagnetic analysis were embedded into a hybrid simulation model, in order to check the coherency between the design and the analysis. The results were coherent.

ÖZET

Bu tezde yapılan deneysel amaçlı bir "tekerlek-içi motor" prototipidir. Tekerlek-içi motorlar 4 tekerlekten bağımsız çekişli elektrikli taşıtlarda kullanılır. Bu araçlarda her tekerleğin içine 'doğrudan-sürüş' yapısında birer tekerlek-içi motor yerleştirilir. Merkezi güç birimli yapıların aksine bu taşıtlarda güç, tork ve hız her bir tekerleğe kontrollü bir biçimde bağımsız olarak sağlanabilir.

Bu tezin içerdiği farklılıklardan birisi şaft eksenine dik, yani radyal, yükleri kaldırabilen doğrudan-sürüş yapısında bir elektrik motorunun tasarımıdır. Tasarlanan motor türü literatürde terslenmiş motor, ya da dış rotor tasarımı şeklinde geçmektedir.

Tasarım temel olarak 'Anahtarlamalı Reluktans Motor' tipindedir. İlk olarak mekanik tasarımın parçası olarak 3-Boyutlu katı modeller yaratılmış, ve gerekli dayanılılıkta olup olmadıkları sınanmıştır. Eş zamanlı olarak elektromanyetik tasarımın da sonlu-eleman-analizi yürütülmüş, gerektiği zaman her iki tasarımda yenilenerek sonuçta birbiriyle tutarlı boyut ve özellikler elde edilmiştir.

Son olarak elektromanyetik analizden edilen veriler melez bir simulasyon modeline girilerek tasarım ve analizin sonuçaları karşılaştırılmıştır. Sonuçlar tutarlıdır.

“for GONDOR…”

ACKNOWLEDGEMENTS

At the beginning, even though I was aware of it, I never thought I'd be this much into this concept. Professor Asif Sabanovic gave me the inspiration and the encouragement for it. He connected me to the experienced academicians from Kocaeli University, and supported me all the way. For his help, I would like to thank him from the bottom of my heart.

I also owe my thanks to Kocaeli side of the project. Professor Feriha Erfan Kuyumcu and his assistants Kadir Yılmaz, and Aytaç ccc helped me for weeks and weeks on this project. I would like to thank them for sharing their Fridays together with me on Maxwell.

My father, Hüseyin Çakır, spent his time and money on producing some of the parts for the motor. Thank you.

Special thanks to Feriha Sertçelik Birol from Arçelik R&D for supplying me the silicon steel rolls for free and helping me on the concept.

Finally, I would like to thank my friends; mechatronics assistants and LFI guys for making life enjoyable to me whenever I was down.

TABLE OF CONTENTS

LIST OF TABLES

LIST OF FIGURES

TABLE OF SYMBOLS

A_s	:	Specific loading (A-turns/m)
A_v	:	Vehicle's frontal projection area (m)
B	:	Flux density (Weber/m^2 = Tesla)
b_{sr}	:	Stator yoke thickness (back-iron)
b_{sy}	:	Rotor yoke thickness (back-iron)
C_d	:	Air-drag coefficient
Error! Objects cannot be created from editing field codes.	:	Bore diameter (mm)
D_o	:	Rotor outer diameter (mm)
D_s	:	Shaft diameter (mm)
D_{wire}	:	Magnet-wire diameter (m)
i	:	Current (A)
I_p	:	Peak current (A)
I_{RMS}	:	RMS current (A)
F	:	Force (N)
F_{air}	:	Air-drag (N)
F_{N_tyre}	:	Normal force acting on a tyre (N)
F_{roll}	:	Friction force due to the rolling (N)
H	:	Flux intensity (A/m)
h_{cs1}	:	Height of winding clearance from the top of the pole (m)

h_{cs2}	:	Height of winding clearance from the bottom of the pole (m)
h_r	:	Rotor pole height (m)
h_s	:	Stator pole height (m)
k_d	:	Duty ratio
k_e	:	Efficiency
L	:	Inductance (H)
Error! Objects cannot be created from editing field codes.	:	Air-gap thickness (mm)
L_s	:	Stack length (m)
L_{aa}	:	Self inductance (H)
L_{ab}	:	Mutual inductance between phase a and b (H)
n	:	Safety factor
P_d	:	Power developed (W)
P_r	:	Number of rotor poles
P_s	:	Number of stator poles
R	:	Resistance (Ω)
R_s	:	Phase resistance (Ω)
R_{wire_m}	:	Magnet wire resistance per meter (Ω/m)
T	:	Torque (Nm)
T_e	:	Electromagnetic torque (Nm)
T_f	:	Fall time (s)
T_{ph}	:	Number of coil turns per phase
v	:	Vehicle speed (m/s)
W_c	:	Co-energy (joules)
w_{coil}	:	Width of the coil (m)
w_{sp}	:	Stator pole width (m)

λ	:	Flux-linkage (V/s)
ϕ	:	Flux (weber)
μ_r	:	Rolling friction coefficient
τ	:	Shear stress (N/m^2)
σ_y	:	Yield stress (N/m^2)
ω_n	:	Rotor speed (rad/s)

TABLE OF ABBREVIATIONS

ABS	Anti Blockage System
EV	Electric Vehicle
FEA	Finite Element Analysis
SRM	Switched Reluctance Motor
VRM	Variable Reluctance Motor
ZEV	Zero Emission Vehicle

1 INTRODUCTION

Throughout the history of transportation, vehicle propulsion milestones have been few and far between. For thousands of years after the invention of the wheel, human and animal muscles were the “motors” behind every vehicle. In the 19th century, the industrial revolution took a giant leap forward with widespread use of the steam engine to power trains and boats across the world.

By the end of the 19th century, two new engines had begun to emerge: the electric engine and the internal combustion engine. Though clean and quiet, electric vehicles lacked the performance and range of machines powered by the internal combustion engine, which quickly came to dominate the automobile industry. In the decades to follow, electric engines were used only sparingly in such vehicles as forklifts, streetcars and golf carts.

As petroleum supplies dwindled and pollution increased in the 1960s and 1970s, the transportation and fuel industries began to re-examine the electric motor. Today, numerous programs are in place to investigate a number of alternative vehicle solutions, with a heightened interest in the clean, efficient capabilities of electric power. [1]

1.1 Electric Vehicles

Electric vehicles are simply vehicles which are driven by means of electric motors on the deck. The category generally forks into two as ‘pure EVs’ which have only batteries or fuel cell structures to power the electric motor, and ‘Hybrid vehicles’ which have generally electric storage system plus a combustion engine.

Although there is an ongoing discussion about the fact that if the EVs are really ZEV class structures or ‘elsewhere emission’ structures, the truth is they have no tail pipe emission at all. In that sense they are quite clean compared to the IC engine vehicles. They are also very quiet too. Electric motors are more efficient than the IC

engines, therefore especially with the help of regenerative braking EVs are economic too.

The reason why they are not common today is the capacity and the quality of today's electrical storage means. Battery technology is the bottle-neck of this emerging technology. They have generally quite low energy/mass ratio, therefore a vehicle with a range of 600 km per battery charge has to carry quite heavy package of batteries. In addition to that, batteries of today suffer from their high internal resistance, which makes recharging process quite slow.

Despite these disadvantages, because of the mostly environmental reasons stated above this technology will definitely will over throne the IC engines eventually. Every day researchers come up with new ideas that help EVs improve in performance and quality.

1.2 4-Wheel Independent Drive Configuration

4 wheel independent drive concept is simply the configuration that each wheel on the vehicle is driven by an independent torque source. Power distribution between wheels is known as differential drive theory in the literature.

Theories about differential drive and skid steering go back in the history almost as long as the electric vehicle itself. The Lunar Rover Vehicle [2] was actually an independent drive configuration, with in-wheel motors.

Today the examples have multiplied. Many private companies are working on in-wheel motors. Most of the race-wining solar cars use this technology. Again the mars robot pathfinder was an 6 wheel independent drive configuration.[3]

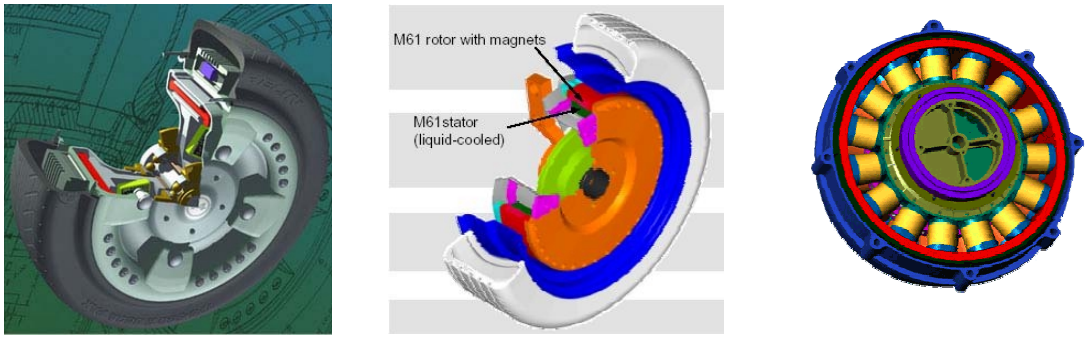

a) b) c)

Figure 1.1 : Examples of some In-wheel Motors; a) TM4, b) MM61, c) Wavecrest Adaptive Motor

Electric motors have many advantages over IC machines. They have fast response, they produce high torques at very low speeds, they are simple and have zero emission.

Having a fast torque response, electric motors are far better controllable then IC engines. If they are fitted inside the wheel of the vehicle, then many things change in today's world of cars.

Differential gear boxes are used in all the cars today. The main purpose of it is to regulate the speed of the driven wheels during cornering. However, although it is a proven concept, it has a weakness. It can only regulate the rotational speeds of the wheels, but not the torque. This drove the manufacturers into very complicated drive assisting equipments for safety and better performance on cars. ABS,EPS,ASR Torsen differentials are some of the technologies emerged to control the traction of a car, they are sophisticated technologies.

An in-wheel motor ends all this mess. Having an direct drive electric motor inside each wheel, eliminates many of the conventional modules in the car; gearbox, differential box, drive shaft, and IC engine of course. The figures below shows how it can change the concept of automotive industry.

a) b)

Figure 1.2 : An Example of how In-wheel Motor concept can revolutionize the vehicle design concept; a) Conventional 4 Wheel Drive Vehicle, b) New configuration using Wavecrest Adaptive In-wheel motors

GM Hy-wire concept utilizes in-wheel motors. In this prototype everything that has anything to the with pushing the car is fitted inside the lower deck of the vehicle. This leaves a very large unused empty space ready to be re-utilized.

a)

b)

c)

d)

Figure 1.3 : An Example of how In-wheel Motor concept can revolutionize the vehicle design concept; a) & b) GM HyWire concept, c) & d) GM Autonomy concept

Of course there's more about this concept then meets the eye. Having the driving torque directly on the road by eliminating all the gearbox and transmission, power loss is decreased quite a big amount. Moreover, regenerative breaking can be utilized more efficiently, since each wheel can be commanded independently. This concept also adds to the safety of the vehicle since all of those assistive technologies mentioned above can be realized in one unit, the electric motor itself. Since it has the ability to generate negative torque, it has a natural ABS ability along with the others.

Because of these reasons stated above this is quite likely to become a default configuration for future EV structures.

2 SRM

The abbreviation SRM stands for ‘Switched Reluctance Motor’. Another widely used term for this motor is VRM; ‘Variable Reluctance Machine’

Reluctance motors were the earliest motors to be developed in the history. Their origins lie in the horse hoe electromagnet of William Sturgeon (1824) (Sturgeon ,W. :’Improved Electromagnet Apparatus’) and the improved version of Joseph Henry and in attempts to convert to ‘once only’ attraction for an iron armature into oscillatory or continuous motion.

Many early designs were reluctance motors and these were strongly influenced by the steam engine, with electromagnets, armatures and current switching arrangements being regarded as the electromechanical equivalents of cylinders, pistons and valve gear.

The first use of the term switched reluctance motor appears to have been by S.A. Nasar (1969)

2.1 Basic Principles of SRM

Variable-reluctance machines (often abbreviated VRMs) are perhaps the simplest of electrical machines. They consist of a stator with excitation windings and a magnetic rotor with saliency. Rotor conductors are not required because torque is produced by the tendency of the rotor to align with the stator-produced flux wave in such a fashion as to maximize the stator flux linkages that result from a given applied stator current.

Although the concept of the SRM (VRM) has been around for a long time, only recently have these machines begun to see widespread use in engineering applications. This is due in large part to the fact that although they are simple in construction, they are somewhat complicated to control. For example, the position of the rotor must be known in order to properly energize the phase windings to produce torque. It is only

relatively recently that the widespread availability and low cost of micro and power electronics have brought the cost of the sensing and control required to successfully operate VRM drive systems down to a level where these systems can be competitive with systems based on dc and induction-motor technologies.

Variable-reluctance machines are often referred to as switched reluctance machines (SRMs) to indicate the combination of a VRM and the switching inverter required to drive it.

A reluctance machine is an electric machine in which torque is produced by the tendency of its movable part to move to a position where the inductance of the excited winding is maximized. This torque is called reluctance torque since it can be said it is out of a tendency to decrease the reluctance to its minimum.

In a simple machine the coil inductance L varies with rotor position θ as shown in Figure 2.1. Assume that the rotor carries a constant current. The positive motoring torque is produced only while the inductance is increasing, and that happens as the rotor approaches the aligned position. Passing the aligned position and entering a decreasing inductance profile, the attractive force between the poles produces a negative torque. If the machine rotates with a constant current in the coil, the negative and the positive torque impulses cancel, and therefore the average over a complete cycle is zero. To eliminate the negative torque impulses, the current must be switched off before entering the decreasing inductance zone. The ideal current waveform is therefore a series of pulses synchronized with the rising intervals.

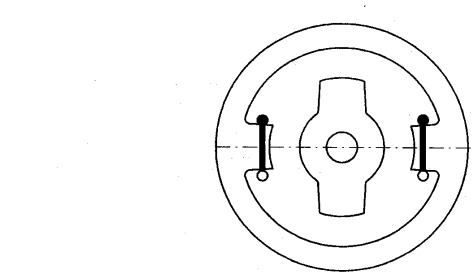

Fig. 3.3 Unaligned position.

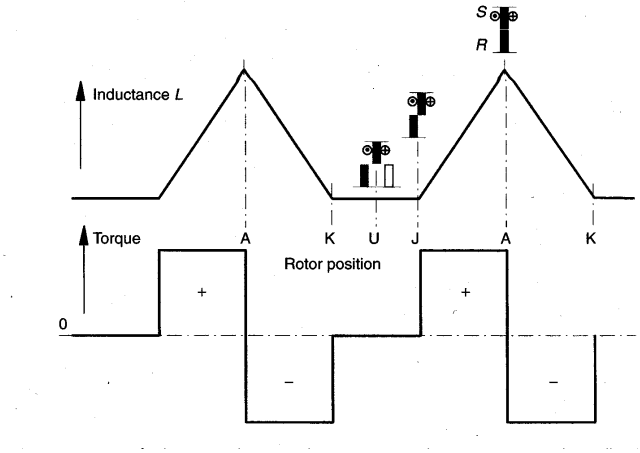

Figure 2.1 : Variation of inductance and torque for constant current with rotor position

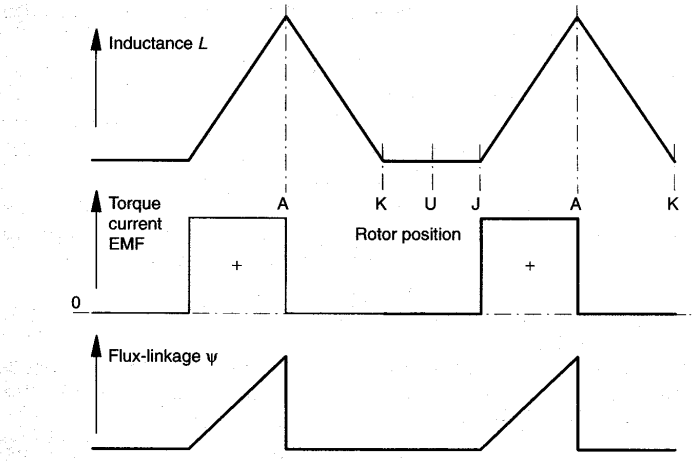

Fig. 3.5 Variation of inductance, current, flux-linkage, torque, and EMF with rotor position, with ideal pulsed unidirectional current.

Figure 2.2 : Variation of inductance current, flux-linkage, and EMF with rotor position

The cycle of torque production associated with one current pulse is called a *stroke*.

There are two main approaches for the mathematical formulation of the produced torque. They are linear and nonlinear analysis.

Linear analysis assumes that the inductance is independent of current (in fact they are dependent): that there is no magnetic saturation (see B-H curve in appendix for M19 electric steel).

Generally mutual coupling between phases is normally zero or small, and is ignored. The voltage equation for one phase is

$$v = Ri + \frac{d\psi}{dt} = Ri + \omega_n \frac{d\psi}{d\theta} \tag{2.1}$$

$$v = Ri + \omega_n \frac{d(Li)}{d\theta} = Ri + L\frac{di}{dt} + \omega_n i \frac{dL}{d\theta} \tag{2.2}$$

Where v is the terminal voltage, i is the current, ψ is the flux-linkage in volt-seconds, R is the phase resistance, L is the phase inductance, θ is the rotor position, and w_n is the angular velocity in rad/s.

The instantaneous electric power is

$$vi = Ri^2 + Li\frac{di}{dt} = Ri + \omega_n i^2 \frac{dL}{d\theta} \tag{2.3}$$

The rate of change in magnetic energy stored is

$$\frac{d}{dt}\left(\frac{1}{2}Li^2\right) = \frac{1}{2}i^2\omega_n \frac{dL}{d\theta} + Li\frac{di}{dt} \tag{2.4}$$

The mechanical power conversion $P = \omega_n T_e$ is what is after resistive loss and magnetic stored energy is eliminated from instantaneous power. Then the torque is

$$T_e = \frac{1}{2}i^2 \frac{dL}{d\theta} \tag{2.5}$$

This equation illustrates an important characteristic of variable-reluctance machines. Notice that the torque is proportional to the square of the phase currents and that as a result it depends on only the magnitude of the phase currents and not on their direction. Thus the motor drive which supplies the phase currents can be unidirectional, i.e., it is not required to supply bidirectional currents. Since the phase currents are typically switched on and off by solid-state switches such as transistors or thyristors and since each switch need only handle currents in a single direction, this means that the motor drive requires only half the number of switches (as well as half the corresponding control electronics) that would be required in a corresponding bidirectional drive. The result is a drive system which is less complex and may be less expensive.

Another fact about the machine is the mutual coupling between phases. In that point of view equation for all phases can be expressed as

$$[v] = [R] \cdot [i] + \left[\frac{d\psi}{dt}\right] = [R] \cdot [i] + [L] \cdot \left[\frac{di}{dt}\right] + \omega_n [i] \cdot \left[\frac{dL}{d\theta}\right] \tag{2.6}$$

For a regular pole winding SRM mutual couplings are generally quite insignificant with respect to self inductances (see Figure 4.33) therefore they are generally ignored. Besides the pole winding configuration generally requires that only one phase is active in a stroke, and this cancels the mutual couplings effects in torque production. There are efforts to utilize the contribution of mutual inductances. Those machines are called 'mutually coupled winding SRM'. In this type of SRM generally two phases are excited at the same time an the torque produce is expressed as

$$T_e = \frac{1}{2} i_a{}^2 \frac{dL_{aa}}{d\theta} + i_a i_b \frac{dL_{ab}}{d\theta} + \frac{1}{2} i_b^2 \frac{dL_{bb}}{d\theta} \tag{2.7}$$

Where i_a and i_b are the current of phases a and b, L_{aa} and L_{ab} are the self and mutual inductances. [MEKROW]

Those linear approaches are valid only to a certain value, that the linearity between flux-linkage and current is cease to exist. Figure below shows an example of this situation.

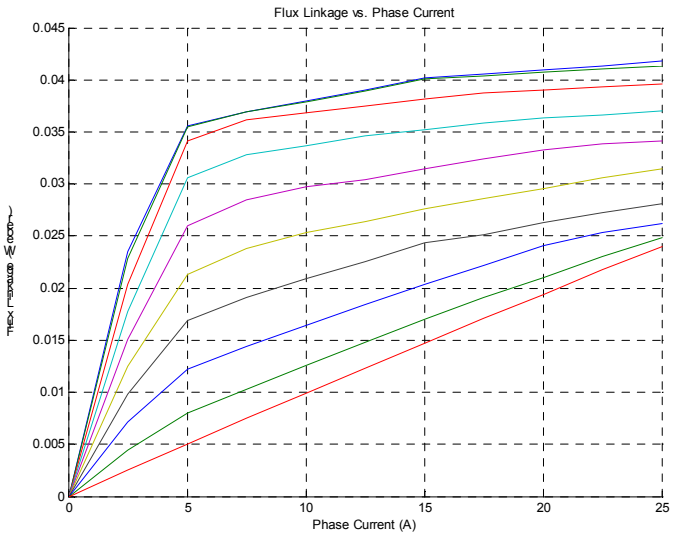

Figure 2.3 : Example of saturation phenomenon

In this situation the torque can be calculated via

$$T_e = \frac{\partial W_c}{\partial \theta} \tag{2.8}$$

where W_c is the co-energy which is defined as in the figure

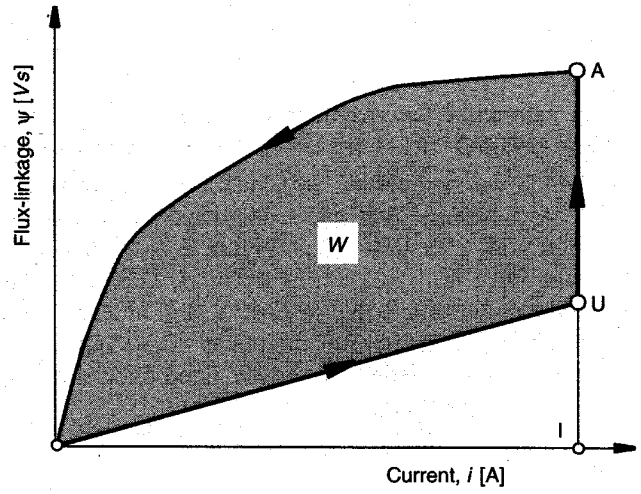

Figure 2.4 : Co-energy

2.2 Why SRM

As it was stated before SRM is the simplest machine in the industry, especially by means of manufacturing. It has rotor and stator just from lamination. The rotor which is the moving part in the machine has no winding at all, this makes is quite easy to apply cooling since cooling the stationary stator is easy. This simplicity property was the main factor that leaded to the selection of producing this type as a prototype.

In addition to that the machine is fault tolerant. As the number of phases increased even though one of the phases is gone it can still keep functioning. That property makes it a very preferable choice for aircraft and aerospace applications.

Generally the necessity of electronic commutation was used to be taken as a disadvantage for this machine, but with today's microcontrollers and power transistors it is no big deal at all. One thing about this matter is the fact that the rotor position has to be known. A mechanical rotary sensor can be used but a sensorless method would be much better. That part of this literature on SRM is still developing.

Torque output of the SRM has big ripple. This could be a problem for a direct drive application generally. However as an in-wheel motor machine will be mounted to

a vehicle, and the equivalent inertia of this vehicle will make a huge fly-wheel effect and this will render this problem insignificant for the performance of the car.

3 PROBLEM DESCRIPTION

3.1 Physical Constraints

The motor in the focus of this material is in-wheel motor. It will be placed inside the wheel. Therefore, its overall dimensions are limited with the empty space available inside the wheel. The cross-sectional view of a standard wheel in Figure 3.1 may give a pretty good idea about the problem.

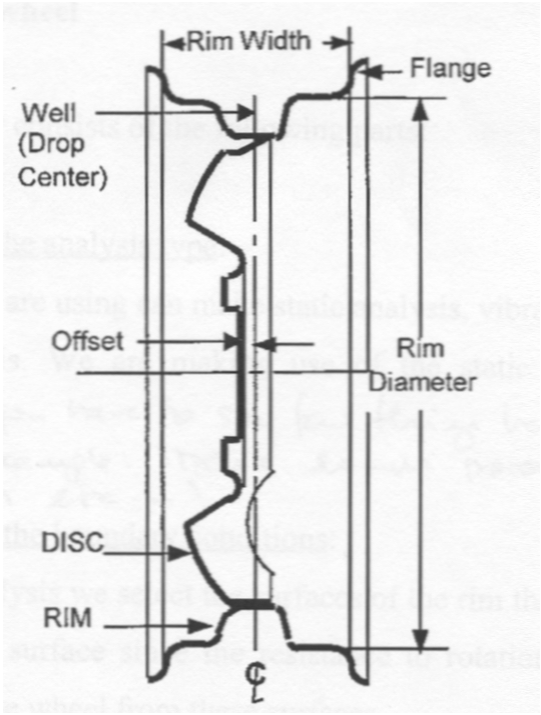

Figure 3.1 : Sectional view of an automobile wheel

Diameter-wise, because of the gnarled and wavy profile of the cross-section, generally for most of the wheel types only 80% of the diameter is available for insertion. There are efforts to increase this value with the help of new generation wheels. One of them is Michelin Pax system. This system was originally developed as zero pressure technology for puncture proof capability. However, because of its small

tire wall thickness and increased inside space made it quite popular for researchers working on in-wheel motors. The fact is that the diameter is everything in this ongoing research and since the torque produced is proportional to the radius, big space means higher torque values.

For class-A, light weight cars, generally R13 and R14 size wheels are used by the manufacturers. These are equal to wheel diameters of 13" and 14". In this case a standard R14 size wheel is used, and the available diameter for this wheel is measured as 29 cm. Therefore the outer diameter of the designed motor will be taken as such.

Another constraint is the width of the available space inside the wheel. This is another parameter that effects the torque output of the system, since it constraints the maximum stack size that can be used. Moreover, strength-wise, that width represents the strength limits of the parts on vehicle's side. Fastening on the knuckle of the car, where the wheel shaft is connected, must have been designed within a moment limit that it can carry. That moment is created by the loadings on the wheel (see Figure 3.2) and is directly proportional to the moment arm length, which in this case the shaft length. Therefore, when designing the shaft that maximum length must not be exceeded. Another issue about this length is that, it is an important parameter for the driving characteristics of the vehicle also. Changing it may result in higher scrub radius, and some other unexpected behaviors.

In the end, under these circumstances it is decided that the shaft length will not exceed 16 cm.

3.2 Mechanical Constraints

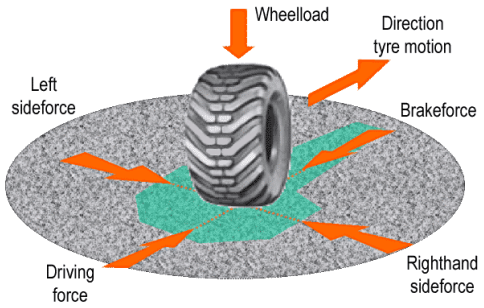

Figure 3.2 : Forces acting on a tire

The motor in subject of design will be placed inside the wheel. Therefore, it must be able to withstand the every force that may act on a vehicle's tire. These forces are visualized in Figure 3.2.

Left side and right side forces are called lateral forces, while the brake force and the driving force are called longitudinal forces. These are important, because they are dependent. The magnitude of total traction a tire can supply is limited and is a function of vertical loading, road surface characteristic, and contact patch profile. This traction is shared between lateral and longitudinal tractions. If one of them, say longitudinal (such as in hard braking) uses up all the available traction, then since there is no lateral traction available the vehicle starts to skid towards the sides. This property is often visualized as a traction circle, but actually it is an offset ellipse.

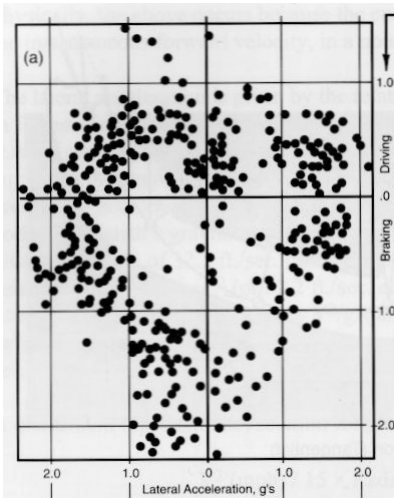

Figure 3.3 : An example gg data for a grand prix car

Figure 3.3 shows the data captured in a grand prix car. On the figure traction circle can be clearly seen. A useful data that this figure reveals is that the tires have different traction capabilities during acceleration and deceleration. Because of the contact patch profile change during deceleration, braking has always a better performance. The data in the figure reads that for forward acceleration the traction value is upper bounded with 1g, whereas for braking this climbs up to 2g. Again for the cornering limits traction can be taken up to 2g also.

Another important data source can be the data supplied by a major sensor company, Kistler. The data supplied by the company belongs to a Class C car (mid-size) can be very useful to have an idea about the forces acting on a tire.

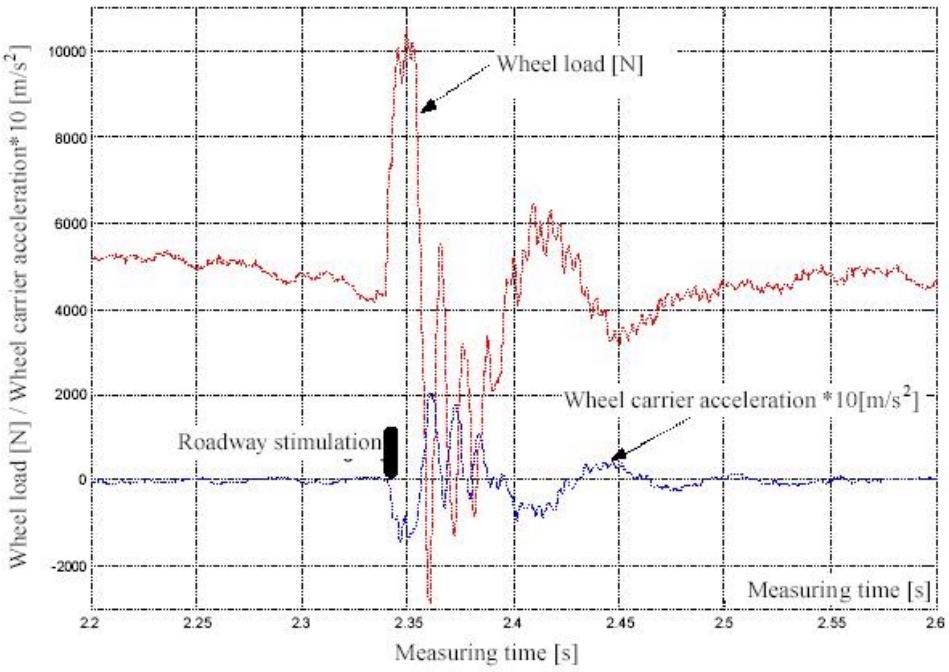

Figure 3.4 : Wheel load measurement (Kistler data)

Figure 3.4 gives some very helpful information about the wheel load values may arise during driving. This data shows that on a bumpy road the vertical loads may climb up to10000N. And there are reasons to believe this is nothing at all. If you think about just a 4cm bump idealized in a triangular shape (to ease the calculations) may result in a vertical acceleration of 20000 m/s^2 ($\cong$ 2000 g) for the velocity of 100km/h, it would be much easier to think about multiple times this value, 10000N. Nevertheless, those conditions are impact conditions and handled different than static analysis. Therefore, it is not necessary to go for numbers like 50kN-90kN.

Another thing that may help for getting a realistic number for limit condition is weight transfer that will occur during cornering. For a 1250 kg during a sharp cornering, the vertical load can easily climb 50% of the vehicle's weight, which is around 6000 N. And if the road conditions are added to this number, to design the shaft for a vertical load of 12000N seems quite reasonable and safe. (safety factor=2)

Yet again, that is not all. Another thing that needs to be handled is the moments that may be acting on the tyre. Figure 3.5 shows the moments acting in an ABS assisted braking.

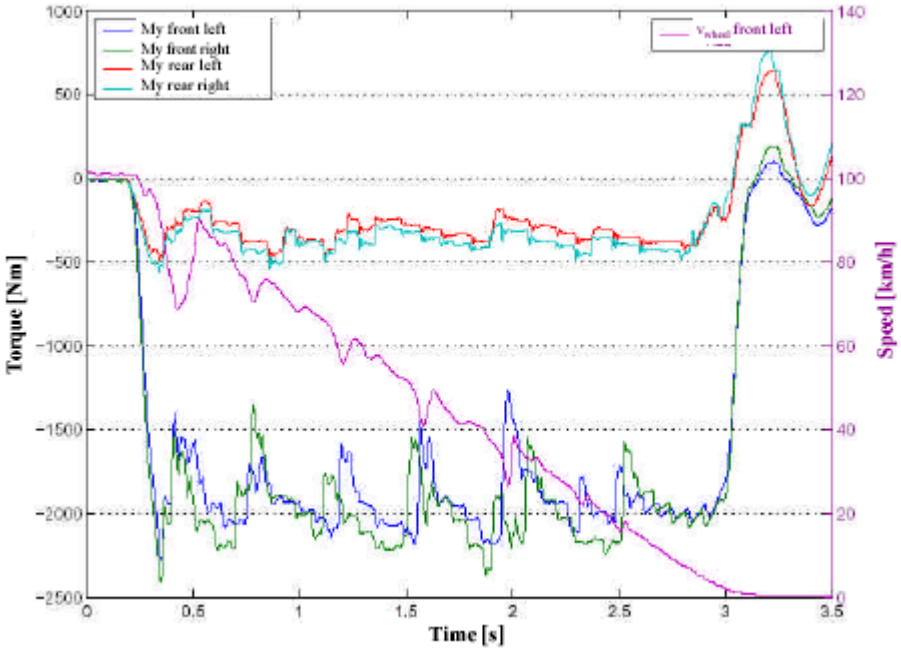

Figure 3.5 : Breaking force distribution on ABS regulating process (Kistler data)

The maximum moment is around 2200 Nm. This reveals another fact about the standard car; that is, since the ABS kicks in around that value, which means the slippage has just started, the maximum traction available is around that number also.

This helps in getting a reasonable moment values that is caused by lateral forces that arise during cornering also. Since it is bounded by the maximum traction available, again that moment can not exceed 2200 Nm.

As a result, design values for braking and cornering is taken as 3000 Nm.

3.3 Electrical Constraints

Although torque is a mechanical concept, the mechanism of torque production explained in this document is electro-magnetic-mechanic energy conversion. Therefore, the question of 'how much torque and power' will be handled in this section rather than in mechanical constraints section.

3.3.1 Necessary Power Output

There exist many resistive forces acting on a vehicle on the move. These are rolling friction, aerodynamic drag force, and internal frictional resistance in moving

parts such as gear boxes, differentials, and bearings. In this document only first two will be taken into account to calculate the necessary power to be developed per motor.

Rolling friction depends on both tire and road surface characteristics, namely the interaction between these two. However, since the tires in focus of this material are conventional types, it can be said that it depends on the road type.

Rolling friction acting on a tire can be calculated as the following;

$$F_{roll} = F_{N\_tyre}.\mu_r \tag{3.1}$$

Of course, this is a quite simple approach, since there are also other more complex theories which include the effects of the rolling speed, and tire pressure as well. Rolling friction coefficients μ_r values can be seen in Table 3.1.

Table 3.1 :Rolling friction values

Road Condition	μ_r **values**
Low rolling friction (good asphalt)	0.008
Normal rolling friction	0.015
Poor rolling friction	0.032
Very poor rolling friction (loose sand)	0.15

Next step is to compute the air drag resistance on the vehicle. Formula for this is

$$F_{air} = 0.5\rho_{air} C_D A_v v^2 \tag{3.2}$$

Again, C_D and A_v values for various models of vehicles already on the market can be seen in Table 3.2.

Table 3.2 : Air drag coefficients

Vehicle (Class)	C_D	$C_D A_v$
VW Polo (Class A)	0.37	0.636
Ford Escort (Class B)	0.36	0.662
Opel Vectra (Class C)	0.29	0.547

BMW 520i (Class D)	0.31	0.649
Mercedes 300SE (Class E)	0.36	0.785

Using these values together with some appropriate tire dimensions and vehicle mass, it is quite straightforward to calculate necessary torque and power as a function of road surface conditions and vehicle speed. A matlab script was written for this purpose (see Appendix) and the output comes out as the following figure.

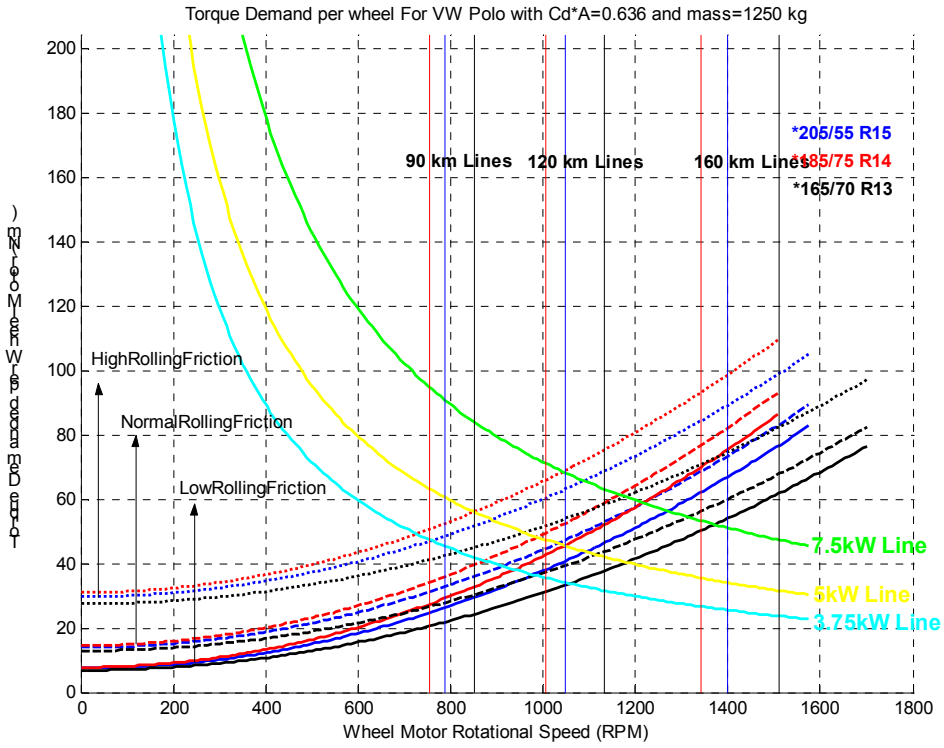

Figure 3.6 : Power & Torque demand per wheel

Looking at the Figure 3.6, one can easily state that under normal rolling friction conditions and using 185/75 R14 type tires, 2.5kW per wheel will be enough to reach a top speed around 90 km/h on a flat road. That also means that the in-wheel SRM has to be able to give a torque output of at least 35Nm at 800 rpm. The reason why 90km/h is selected as a target speed is that it's top legal speed in most of the countries all around the world.

4 DESIGN PROCESS

Design process includes mechanical design, electromagnetic design, and heat transfer design. These are placed successively in the chapter. However, reader must be aware of the fact that this work is iterative in nature. Although they are placed in order, that does not mean that the real design followed the same route; in fact it did not. Many times through out the process deciding on a dimension might need a parameter that can not be known exactly before that dimensioning part is over. Again, sometimes deciding on a parameter could render another part of the design inappropriate. Because of these reasons, it's quite likely to find back and forth references in the following topics, which may be confusing to the reader. Whole design was converged into a set of parameters after several tries and iterations, but here it will only be placed the last one.

4.1 Mechanical Design

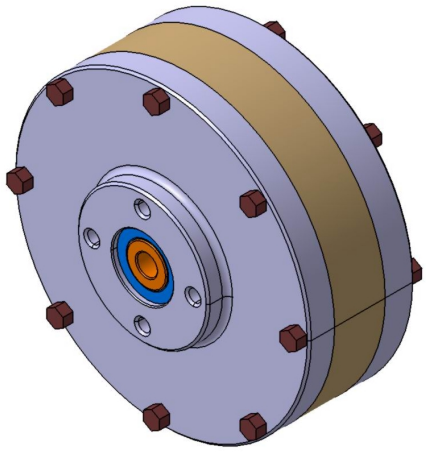

Figure 4.1 : 3D model of In-wheel motor

The product of this project is not a commercial product. Not in any part of the documentation no effort has been made to sculpt the product into a more aesthetic look. The machine will be a first iteration of new designs, and most probably will be

subjected to many modifications partially or totally. Therefore the machine is designed quite ‘serviceable’. It means that to assemble and disassemble it will be easy. Again since it is an experimental early prototype no effort has be made to design it for minimum weight also. Front and rear disk will be aluminum alloy, while the two bushings inside can be out of thermal plastics of aluminum again. The shaft is carbon steel, and the magnetic laminations are silicon steel of M19 (M230-50A).

4.1.1 Shaft

Generally hub design is one of the most critical parts of the vehicles. They must withstand all the load conditions a vehicle can undergo. In this case it was the same.

Shaft design for the motor does not differ too much from a classical hub shaft of vehicles on the market. On difference is that in general conventional hub shafts have a conical or tapered shape. This is optimum design in order to withstand the increasing stress towards the inner end of the shaft. In this case, that is not quite applicable, since stator of the motor is composed of laminations, and this stack type formation make it a complicated necessity to design each stack inside diameter separately. Other solution may be utilizing a collar on the shaft to cover the taper. Then again, that will increase the wasted space at the center, which will directly decrease the available space for coils.

The proposed design can be seen in Figure 4.2. Since the motor under design process in the material is for experimental purposes, it is quite important to be able to assemble and disassemble it easily. Tapered bearings suits perfectly for this use (See Figure 4.10). In order to hold the bearings from moving along the force they will be under, this stair-like structure is proposed. Along the axis of the shaft there are four different diameters which were decided iteratively through out the design process in order to meet the desired strength characteristics under the dimensional constraints of the commercially available bearings on the market.

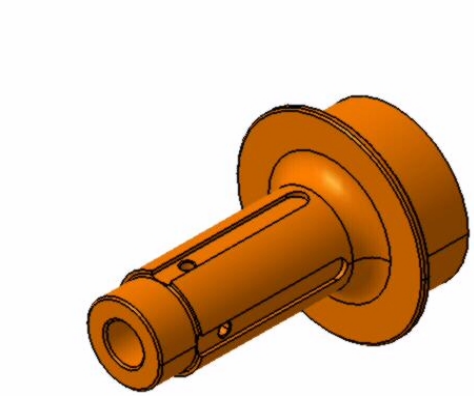

Figure 4.2 : Proposed Shaft Design for In-wheel Motor

The grooves (or key ways) in the design are to transfer the torque to the shaft. This torque can be thought as breaking or driving torque. The inverse profile of these 90° shifted grooves exist on the proposed stack lamination. Therefore, stator can slide on the shaft and can sit there locked on the rotation axis. Again four holes toward the outer edge of the shaft inside the grooves allow the wiring through. Those are placed toward the outer edge, because if they are placed inside, those will act as stress concentration areas and this can cause failure at this most stressed part of the shaft.

4.1.1.1 Loading Condition 1

Examining the Kistler data (see Figure 3.4), it can be stated that shaft must be able to withstand transverse loading more than 11 kN. This can be proved by from another point of view also. Thinking a 1250 kg vehicle in mind, according to driving conditions with the weight transfer phenomena, the transverse loading on one wheel can easily climb up to 40% of vehicle's weight. Together with the road conditions that number and even a higher value seems logical to be taken into account. In this design this value will be taken 14kN.

This force will be shared between the two bearings on the shaft. The question of 'with what percentage' depends on the dimension of the wheel that will be used. Together with the width of the wheel rim, offset value of the wheel affects the value considerably.

Using a wheel type of 175/75 R14 with a negative offset value, sharing can be around 55% for the front side bearing. A finite element analysis was done using this loading condition. (See Figure 4.3)

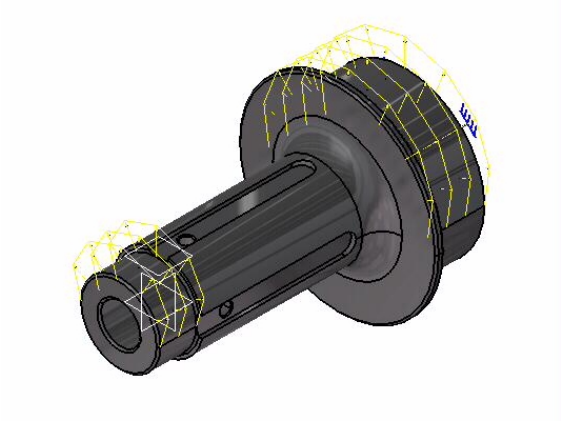

Figure 4.3 : Loading Condition 1

The results of the FEA for loading condition 1 can be seen in Figure 4.4 below. The results consist of meshing on the part, translational displacement vectors, nodal Von Misses stress values, and principle stresses.

Looking at the outputs, shaft stands safe for this loading condition. Some regions on the shaft have fine mesh whereas other regions have coarser. This is because the stress concentration areas needed to be analyzed much more carefully. Therefore, grooves, holes on the grooves, neck regions where diameter changes have locally finer mesh structure. Maximum Von Misses stress value occurs near the large neck towards the end of the shaft and around the groove end, as it was expected. However, the value is not dangerous. For the shaft to be failed, maximum Von Misses stress value has to exceed the yielding stress of the material used. In this case, maximum stress is given as 147 MPa, whereas the yielding stress of carbon steel can be between 200-600 MPa. Therefore, it is safe at this stage.

Another important parameter that has to be taken into account is the displacement. This value is important because the air-gap thickness in the design is 0.4mm. The displacement value at the mid-region of the shaft shows how this thickness changes and if there is any contact. In this case, the mid-region displacement is around 0.04, ten times smaller than the air-gap thickness. That is satisfactory.

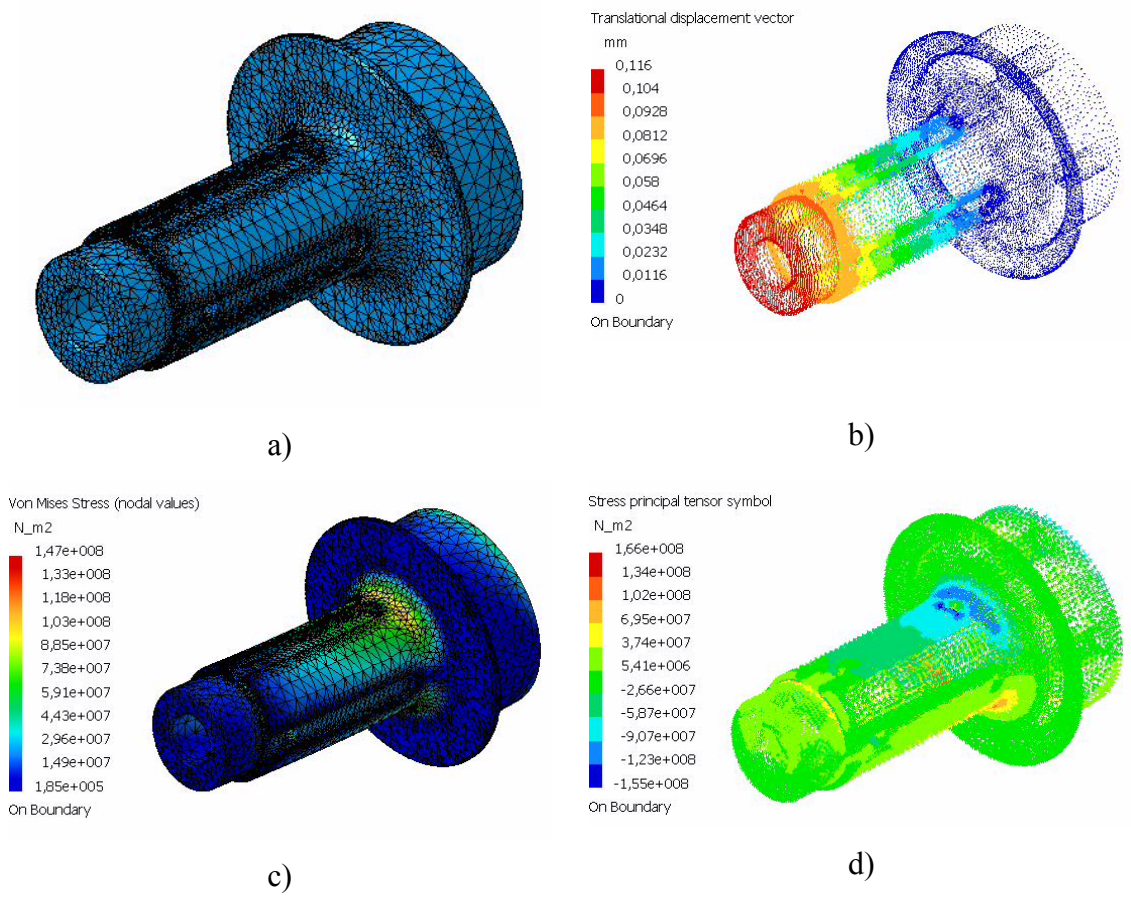

Figure 4.4 : FEA Results for Loading Condition 1; a) Mesh Structure, b)Displacement, c)Von Misses Stress, d) Principle Stresses

4.1.1.2 Loading Condition 2

Another important parameter on the design is the moments that will act on the shaft due to cornering. (See Figure 4.7 a)) That moment is due to the available lateral traction at the moment. In this case, full traction availability is taken into account. This is the case the vehicle is cornering at a speed that causes the vehicle to skid and there is no longitudinal acceleration (If it skids outward the corner it means there is no longitudinal traction available anyway). For a performance car this acceleration can go up to 2g (even higher in Formula1 cars) (see Figure 3.3). This information and remembering the weight transfer phenomenon that was mentioned before can lead to coming up with a moment value of 2000Nm. Figure 4.5 represents this condition.

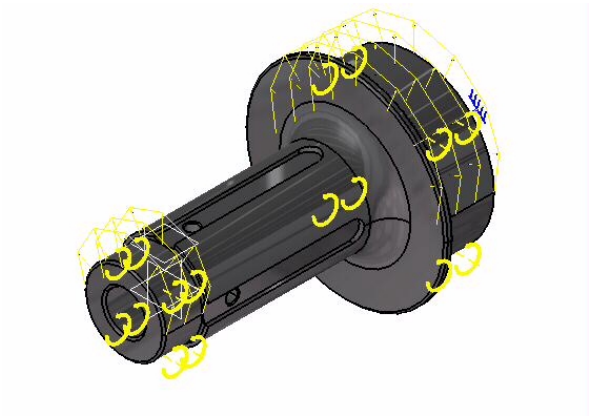

Figure 4.5 : Loading Condition 2

The results of the FEA for loading condition 1 can be seen in Figure 4.6 below.

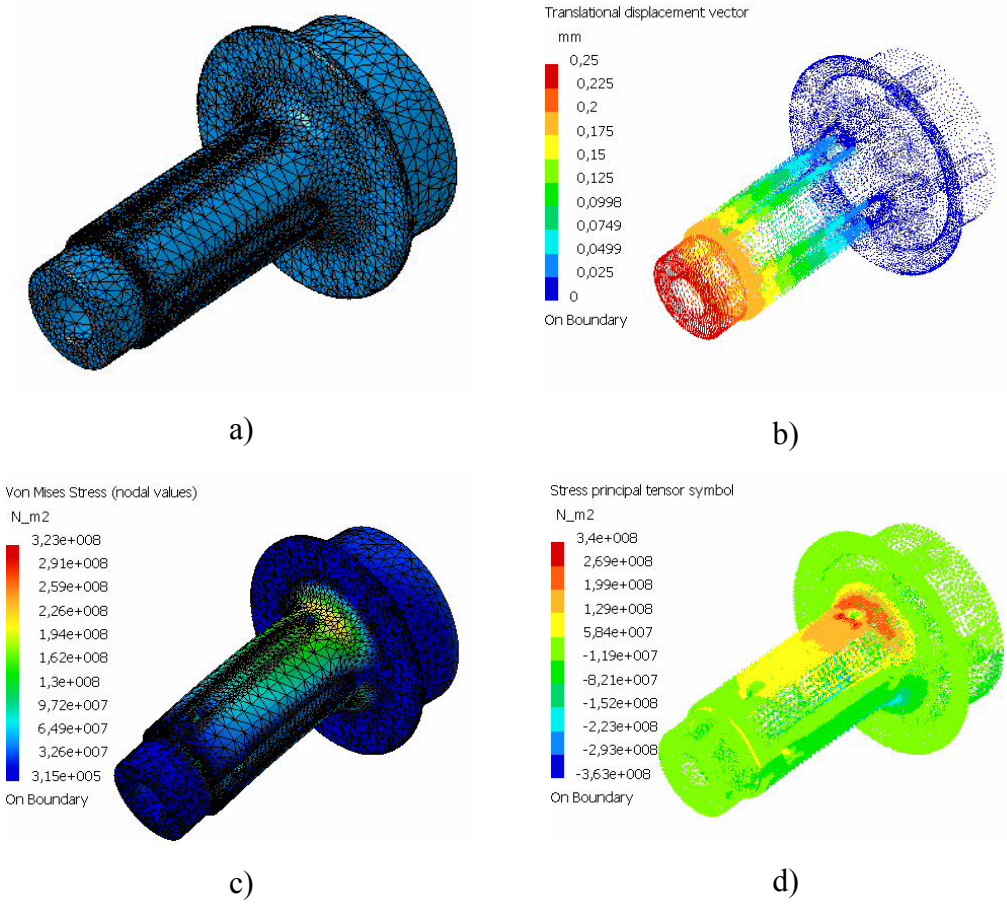

Figure 4.6 : FEA Results for Loading Condition 2; a) Mesh Structure, b) Displacement, c) Von Misses Stress, d) Principle Stresses

Von Misses stress data shows that the shaft is still in safe region. The maximum stress occurs is 323 MPa. Likewise, the displacement data gives a value of 0.099 mm around the interested region. This is safe also.

4.1.1.3 Loading Condition 3

The last loading condition considered is combination of all previous loadings plus brake or drive torque depending on the longitudinal traction available at the moment. The question is which one to use for the analysis; the brake torque or the drive torque. Looking at the gg data (see Figure 3.3), the reader may think that it should be the brake torque that should be considered, since generally the available longitudinal traction at breaking is higher than driving. However, in this case it's a little different. Due to structure of the in-wheel motor, brake torque depends on the torque production capability of the motor, and has nothing to do with the available traction. Even if a mechanical disk brake is added to ensure safety, that will act through the rotor, and the motor can participate this, at most, with its maximum torque output. Therefore, the force acting on the shaft groove will be due to this maximum torque.

a) b)

Figure 4.7 : Loading Condition 3; a) A car cornering, b) Loading on the Shaft

Here, the target design is 35-40 Nm at 800 rpm. Considering the torque versus rotational speed characteristic of the SRM, and with more current boosting for a short time, it's reasonable to think about a maximum brake torque of 110Nm.

This value was reflected as distributed forces acting on the groove walls in the FEA. Due to the nature of the software program that has been used, although there exists no contact on a region 20mm wide at both ends of the groove walls, the forces distributed on the entire wall surface. This has to be remembered while analyzing the results of the FEA.

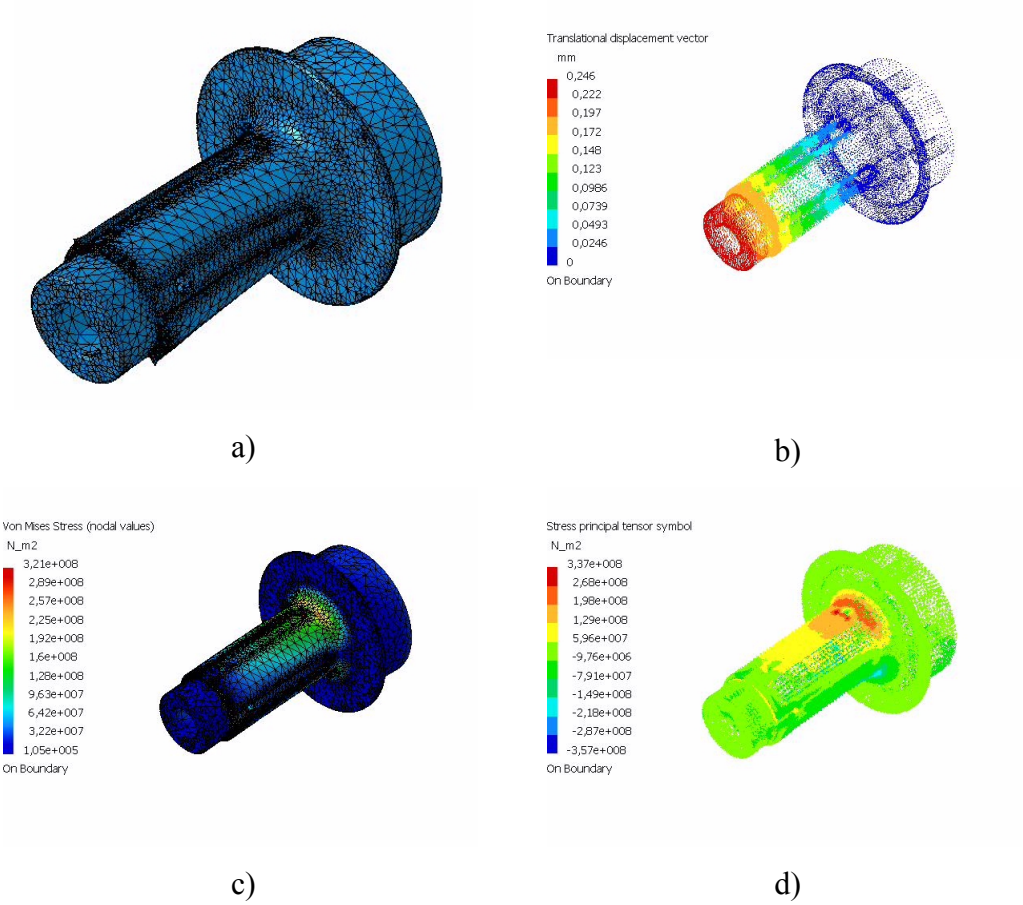

Figure 4.8 : FEA Results for Loading Condition 3; a) Mesh Structure, b) Displacement, c) Von Misses Stress, d) Principle Stresses

Looking at the results it can be clearly seen that the neck region is still dominating by means of stress concentration. Maximum Von Misses stress is 328 MPa and this occurs around the neck not on the groove corners. This magnitude of torque is quite harmless for the design.

4.1.2 Bolts

Another parameter to decide is the bolt diameter that will be used to clamp the front disk, rotor laminations, and rear disk together. It can be fatal because they will be under shear loading due to drive or brake torque. Here, since it's almost clear that target output torque of the machine won't be enough for emergency braking and it will be needed to add mechanical means, a disk break also. In that case, bolts have to withstand this torque's effects.

To be able to claim that the bolt is safe it must satisfy the following condition;

$$\tau < \frac{\sigma_y}{2n} \tag{4.1}$$

where, τ is the shear stress on the bolt, n is the safety factor, and σ_y is the yield stress of the bolt's material.

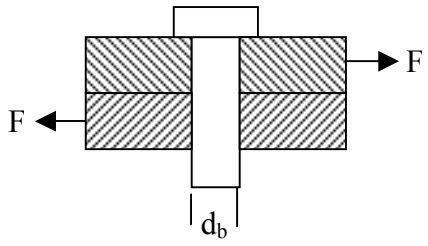

Figure 4.9 : Bolting

Making the calculation accordingly (see Appendix) M10 size bolt will be a safe choice.

4.1.3 Bearing Selection

As it was mentioned before, since easy assembling and disassembling is a desired property in this context, tapered bearings were the natural choice for this mission.

Figure 4.10 : Tapered Bearing

Tapered bearings can take thrust loading in one direction; in fact it is a necessity for them in order to operate properly. Therefore, to ensure that motor can take lateral force in both directions, two of them are used in opposite orientation in face-to-face configuration.

Looking at the loading specifications it was seen that bearings in the range of interest by means of their dimensions were already over-safe to use. Therefore, the main criteria for the bearing selection were the dimensional constraints that came out of the shaft design process, namely the inner bearing diameter and maximum width.

In the end, accordingly SKF 32008-X and SKF32016-X types of bearings were chosen to be used in the design. (see Appendix)

4.2 Electromagnetic

4.2.1 Dimensioning

Flux linkage-voltage relation for a flat-topped phase current can be obtained, by neglecting the resistive voltage drop, as;

$$V \cong \frac{d\lambda}{dt} = \frac{(\lambda_a - \lambda_u)}{\lambda_u} = \frac{(L_a^s - L_u)i}{t} \tag{4.2}$$

and time t can be expressed in terms of stator pole and rotor speed as:

$$t = \frac{\beta_s}{\omega_n} \tag{4.3}$$

If we, for simplicity, define two new parameters as the following;

$$\sigma_s = \frac{L_a^s}{L_a^u} \tag{4.4}$$

and

$$\sigma_u = \frac{L_a^s}{L_a^u} \tag{4.5}$$

where L_a^u is the 'unsaturated phase of aligned' inductance, L_a^s is the 'saturated phase of aligned' inductance, and L_u is the 'unaligned' inductance. Now, applied voltage can be re-expressed in those terms as;

$$V = \frac{\omega_n}{\beta_s} L_a^s i(i - \frac{1}{\sigma_s \sigma_u}) \tag{4.6}$$

Flux-linkage for the aligned position can also be expressed in different terms such that;

$$\lambda = L_a^s i = \phi T_{ph} = BA_{sp} T_{ph} = BDL\beta_s \frac{T_{ph}}{2} \tag{4.7}$$

Here, A_{sp} is the stator pole area, L is stack depth, B is the flux density at the aligned position.

There is also another parameter which may help in the design process;

$$A_s = \frac{2T_{ph}im}{\pi D} \tag{4.8}$$

A_s is called the specific electric loading, here m stands for the number of phases conducting at the same time, which in this work is always 1.

Then comes the most important part; the power developed out of this machine:

$$P_d = k_e k_d Vim \tag{4.9}$$

k_e is the efficiency, it will be taken as 0.85 in this calculation, and k_d is the duty cycle which can be expressed as;

$$k_d = \frac{\theta_i q P_r}{360} \tag{4.10}$$

Combining these, the power developed can be rearranged to give

$$P_d = k_e k_d k_1 k_2 B A_s D^2 L N_r \tag{4.11}$$

where

$$k_1 = \frac{\pi^2}{120} \tag{4.12}$$

and

$$k_2 = 1 - \frac{1}{\sigma_s \sigma_u} \tag{4.13}$$

Having completed the derivations of the necessary equations, now it is time to start the iterative calculations. There are a few parameters that need answering. However, the problem with them is that they can not be known exactly unless the design is over. Therefore, those parameters must be guessed, this is what makes this process iterative and tricky in nature.

Parameter k_2 is related to the different characteristic inductances of the machine. The literature says that in general this parameter can be bounded as the following;

$$0.65 < k_2 < 0.75 \tag{4.14}$$

In this case it is taken as 0.65.

Another parameter that needs initial guessing is the specific electric loading. Again it is stated that it is usually in the range of

$$25000 < A_s < 90000 \tag{4.15}$$

This is where a lot of modifications have been made. At first it feels like having a high specific loading is the best, but after a few iterations it turns out that, for the space available inside the motor, a low value of A_s fits better. It is simply a question of how many number of turns you can fit inside for a specific design current. Then a value of 24000 is found the best.

The duty cycle k_d can be taken 1, since the current conduction angle θ_i is supposed to be maximum 15° for 6/8 machine. The reason behind this is as such; theoretically torque is produced only during an increasing inductance profile and this can occur only while the overlapping angle between the stator and the rotor increases (or decreases). Then another parameter comes on the scene, and that is stroke angle ε. That can be defined as the phase shift between stator phase strokes. It is actually the angle swept during the time between a stator phase is excited and when the time comes to shut it and excite the other one. Stroke angle can be calculated as follows;

$$\varepsilon = \frac{2\pi}{qP_r} \tag{4.16}$$

where $q = \frac{Ps}{2}$. In this case ε is 15°.

This may lead the discussion into a new conclusion. Since for a SR machine with its rotor and stator pole numbers are known, its stroke angle is fixed also. This stroke can be applied only during increased inductance and that puts a lower bound on the stator arc dimension as the following;

$$\min[\beta_s] = \frac{2\pi}{\frac{P_s}{2}P_r} \tag{4.17}$$

In this design of SRM with a 6/8 configuration $\min[\beta_s] = 15^\circ$. Now it is necessary to come up with a number for β_s. It is a dimension that needs to be guessed unfortunately. Guessed and then iteratively correct again and again until it is decided that it converged to an optimum number for the particular design.

There are publications on this matter, and they generally concentrated on a the ratio called ‘Stator Pole Enclosure’. Stator pole enclosure is defined as the ratio of β_s to the pole gap, which is the angle between two successive poles. Then;

$$\beta_s = \frac{2\pi}{P_s} StatorPoleEnclosure \tag{4.18}$$

Krishnan's empirical results haven been used in selection of proper StatorPoleEnclosure value. He claims that generally the best values lie between 0.35-0.45.

Through out the iteration many values have been tested, but for some reason, which will be clearer to the reader in the next few paragraphs, in the end a value of 0.30 was decided. Then β_s becomes 18°.

Having decided the values of β_s, A_s, and k_2, it is all down the hill from now on, if stator bore diameter D is known. D can be calculated using equation 4.11.

Accordingly then, stator pole thickness becomes;

$$w_{sp} = DSin\left(\frac{\beta_s}{2}\right) \tag{4.19}$$

Back-iron thickness for stator and rotor can be limited using some observation. In Figure 4.15 it can be seen that the flux lines fork into two and then enter their path way on back-iron band. Therefore the lower limit should be the width of the flux line, namely the stator pole thickness w_{sp}.

$$w_{sp} > b_{sy} > 0.5w_{sp} \tag{4.20}$$

$$0.5w_{sp} > b_{ry} > 0.75w_{sp} \tag{4.21}$$

After the iteration it is decided that for both b_{sy} and b_{ry} the best value is $0.62w_{sp}$.

Then comes the calculation of stator and rotor pole heights and they are as the following;

$$h_s = \frac{\left(D - D_s - 2b_{sy}\right)}{2} \tag{4.22}$$

and

$$h_r = \frac{\left(D_o - D - 2l_g - 2b_{ry}\right)}{2} \tag{4.23}$$

Another very important dimension that has to be decided on is the rotor pole arc. One can recall that during the shut down phase it is important to kill the phase current before it passes to the negative torque region. Here the rotor pole arc play an important role because for a particular inductance, stator resistance, and DC link voltage, it constraints the maximum amount of time for this killing phase. Therefore, it has to be

decided carefully to avoid undesired negative torque spikes at the designed speed. The lower and the upper bound for this dimension are as the following.

$$\beta_s \le \beta_r \le (\beta_s + \theta_{fr}) \tag{4.24}$$

Here θ_{fr} is called the fall-angle, and calculated as ;

$$\theta_{fr} = \omega_n T_f \tag{4.25}$$

T_f is the fall-time in seconds and can be calculated by solving the differential equation;

$$-V_{dc} = R_s i + L(\theta)\frac{di}{dt} + \frac{dL(\theta)}{dt} i \tag{4.26}$$

The reason why the applied voltage is minus can be found in chapter 2 and section 3.3 of this chapter. Solving this equation for t and with $i(0) = I_p$ (I_p is the peak current), the fall-time is found as;

$$T_f = \tau_a \left[1 + \frac{R_s I_p}{V_{dc}} \right] \tag{4.27}$$

where τ_a is in seconds and;

$$\tau_a = \frac{L_a}{R_s} \tag{4.28}$$

To be able to do the calculations value of stator phase resistance is needed, and for that it is necessary to know the exact coil dimensions. Therefore it is time to go on with that.

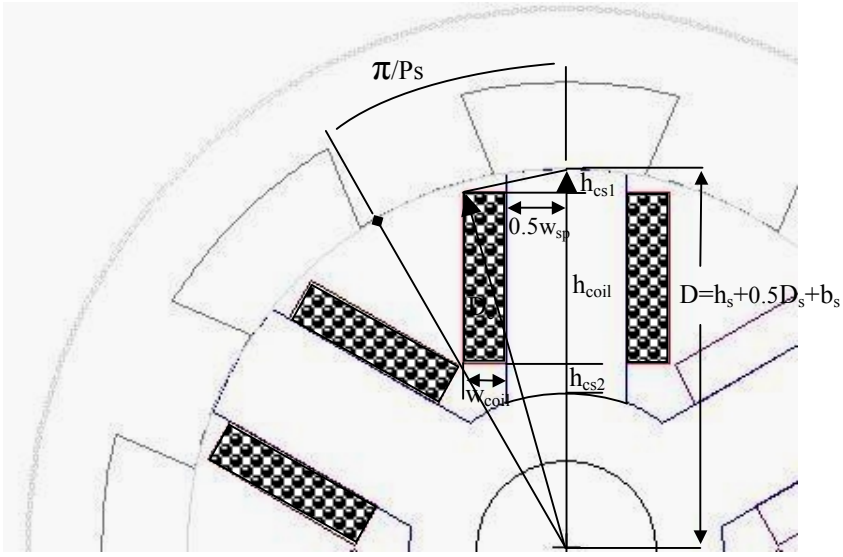

Figure 4.11 : Coil dimensioning

Looking at the Figure 4.11, it is clear that for a cylindrical coil structure maximum coil width can be;

$$\max[w_{coil}] = \tan(\frac{2\pi}{2P_s})(b_{sy} + \frac{D_s}{2}) - \frac{w_s}{2} - 0.002 \tag{4.29}$$

2 mm gap is left a safety tolerance and for heat transfer purposes. Accordingly, upper safety gap height for the coil can be calculated as the following;

$$h_{cs1} = \frac{D}{2} - \sqrt{\left(\frac{D}{2}\right)^2 - (w_{coil} + \frac{w_{sp}}{2})^2} + 0.002 \tag{4.30}$$

This is necessary for the winding not to interfere with the air-gap.

The number of turns per phase for a given power and specific current can be calculated via equation 4.8, but that is not necessarily the number that can fit the space. Proposed layering can be seen in the figure below.

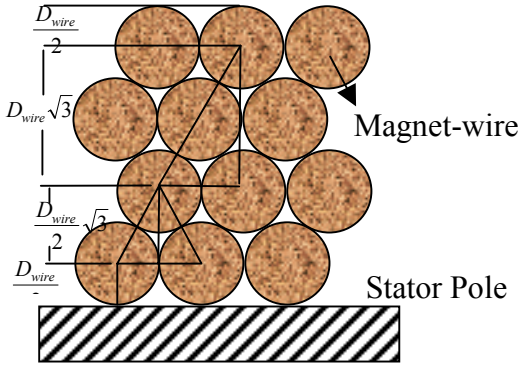

Figure 4.12 : Height of coil

Maximum number of turns per phase that can be fitted inside the motor is given as;

$$\max[T_{ph}] = 2\left(\frac{h_s - h_{cs1} - h_{cs2}}{D_{wire}}\right) * \left(\frac{w_{coil} - D_{wire}}{\frac{D_{wire}}{2}\sqrt{3}} + 1\right) \tag{4.31}$$

Having T_{ph} and using length-wise resistance, R_{wire_m} (Ω/m), of the magnet wire in use R_s can be calculated as;

$$R_s \cong R_{wire\_m} 2(L_s w_{sp}) T_{ph} \tag{4.32}$$

From this calculations with the maximum $T_{ph} = 120$ turns, and $R_{wire\_m} = 2.6 \times 10^{-3}$ Ω/m, R_s is calculated as 0.06 Ω.

Going back; $\theta_{fr} = \omega_n T_f$ can be calculated around 5° for a speed of 900 rpm. According to the equation β_r is decided as 22°.

4.2.2 Maxwell FEA & Simulation

Having completed the dimensioning, the next step is to make the necessary simulations and the analysis for this new designed machine. Maxwell equations and the virtual work method are the theory behind this. Although the Maxwell equations are quite important and useful, there exists a problem that it is not always possible to guarantee to have solution. Moreover, as it was stated before, SRM has a quite nonlinear nature and this makes it extra hard to come up with an analytical solution. In order to overcome this problem numerical methods and finite element tools are utilized many times.

Maxwell 2D of ANSOFT is the software that is used for this purpose through out this work. The main procedure of this part of the works is as the following;

1. Drawing the structure in the drawing module,
2. Assigning the material properties of the materials in the simulation,
3. Assigning the boundaries and the properties of them,
4. Creating a parametric solution table to be followed,
5. Running the simulation
6. Post processing to analyze the results

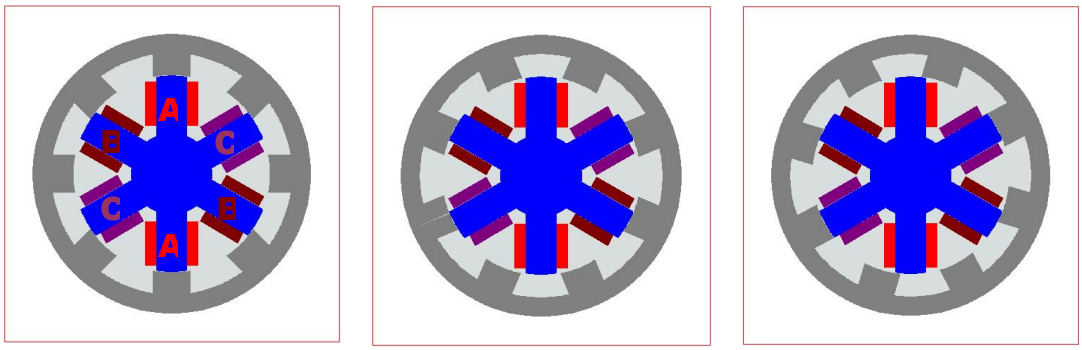

a) b) c)

Figure 4.13 : SRM's three distinctive rotor positions for PhaseA; a) Aligned , b) Unaligned ,c)Aligning just begins

Designed motor is 6/8 type, which means it has 8 rotor poles, and 6 stator poles. As it was mention before generally SR motors have a symmetric topology and this symmetry brings the advantage of periodicity. In this case, since the machine has 8 rotor poles, it has 45° periodicity (or 22.5° half-periodicity). Therefore, a parametric solution that covers the rotor positions of a 45° range will be just enough. For instance, this means that the simulation will start from aligned position of phase A and rotor will be rotated step by step following the parametric table, and it will come to a stop phase A comes to aligned position with the next rotor pole.

In the previous topic base current was designed as 45A, so it is necessary to make sure that the parametric solution covers at least two times of this value for all phases. In this case, it means 90A.

Before running the simulation, it is important to make sure that the mesh structure is suitable for the purpose. In Figure 4.14 reader can see an example mesh used in Maxwell2D. That structure consists of around 8000 triangles and the more than half of these triangles are in the thin air-gap. That is because the air-gap plays a major role in the torque production. In the electromagnetic conversion most of the energy is stored within this thin band. This will be clearer when the results are available.

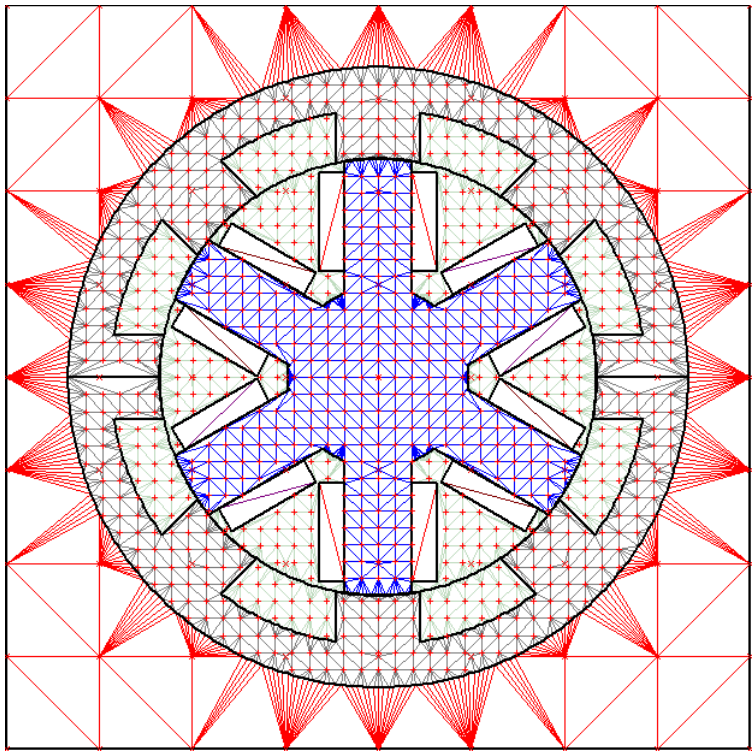

Figure 4.14 : An example of Maxwell2D mesh for SRM model

Below in Figure 4.15 one of the result of the simulation can be seen. It is the flux linkage values for different positions at 45 A with phase A excitation.

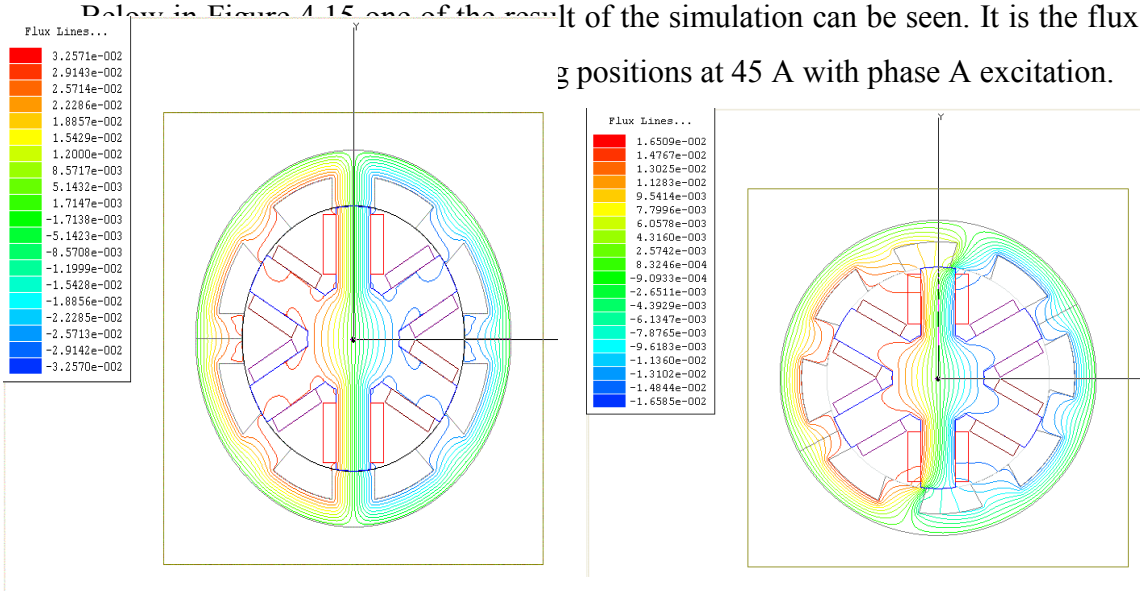

a) b)

Figure 4.15 : Flux line distribution with 45A phase A excitation; a)Aligned , b) Overlapping begins

The results are coherent with the theory, and show that torque production is possible. Of course, there exist some flux paths not obeying the mainstream. That was also expected and this is called ‘the leak’. That is one of the factors which degrade the efficiency of the motor. It can be diminished, but never can totally be killed.

Next results are the flux density (B) and the flux intensity (H) field graphs

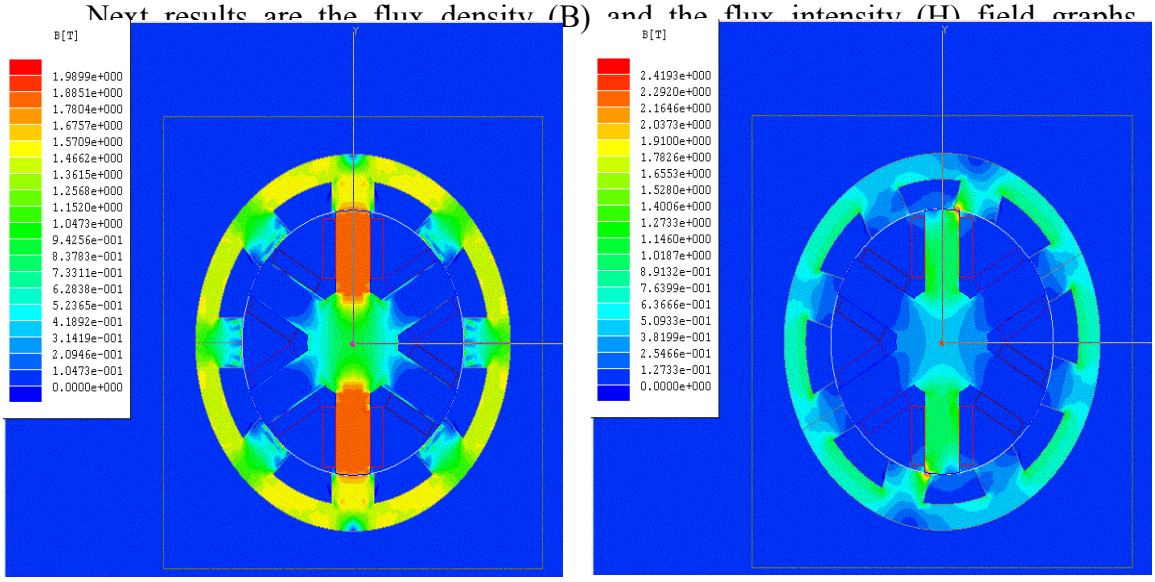

a) b)

Figure 4.16 : Flux density (B) with 45A phase A excitation; a)Aligned , b) Overlapping begins

They are both reasonable also. Looking at B graph, it can be seen that maximum values are within the coil region and air-gap. Also for the one in which the overlapping begins, contact zone has the maximum values. Flux path just finds a narrow way through, and flows in. Since the cross sectional area at the moment is small for the flux magnitude, B increases significantly in that zone. Another thing is that the maximum value of the B is given as 1.9 Tesla in the result. That shows that taking a value of 1.7 Tesla for B during the process of dimensioning was not that bad at all.

And for the flux intensity H, it can be seen that the maximum magnitudes are within the air-gap band, where the permeability is small. This is another prove of why

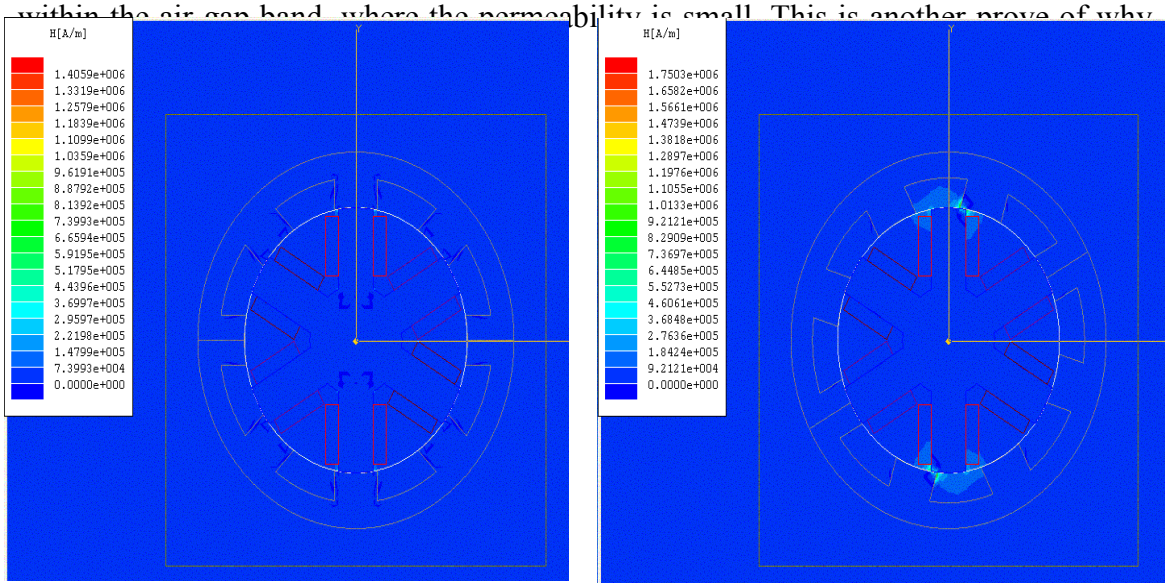

a) b)

Figure 4.17 : Flux intensity (H) with 45A phase A excitation; a)Aligned , b) Overlapping begins

The next plots in this section have been generated by Matlab using the simulation outputs. First one is the flux linkage plot. There, it shows the flux linkage versus phase current A for different rotor positions between 0°-45°, namely the two aligned positions.

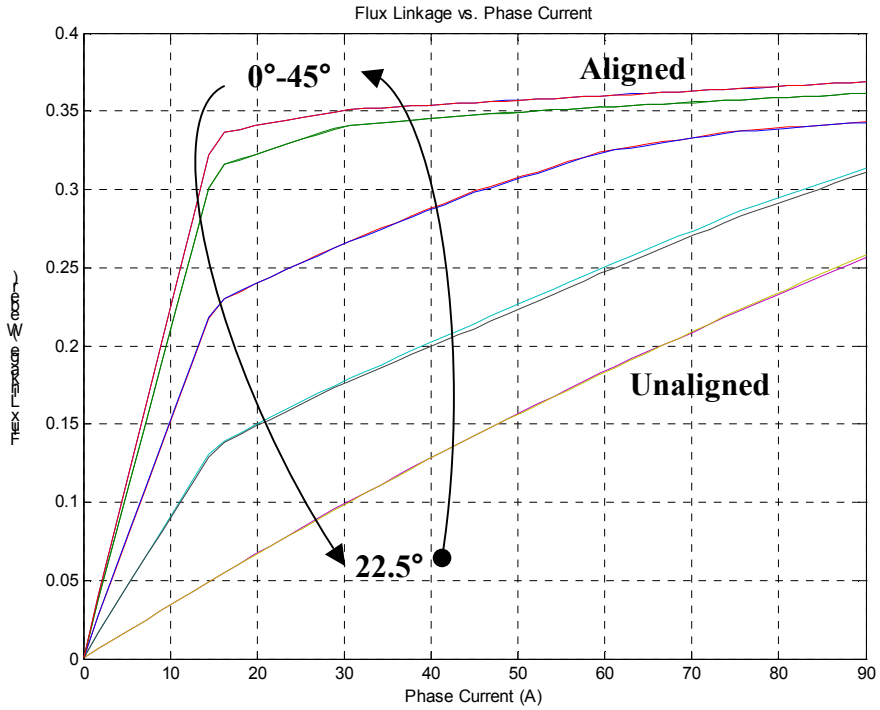

Figure 4.18 : Flux Linkage vs. Current for phase A between 0°-45°

Saturation effect is quite obvious in the graph. After the current value of 15A medium starts to saturate and the inductance decreases significantly.

As for the inductances, results are problematic. Theoretically, around 0 and 45 a flat inductance region should exist. This is dead region for torque production and can be used to kill the current in the coils before decreasing inductance profile starts. In this case the profile is like a triangle and there is no dead zone. This would probably will cause a instantaneous torque drop while trying to kill the current.

The mutual inductance can be seen in the next figure also. The magnitudes show that, as it was stated theoretically, they are insignificant with respect to self inductances. Therefore even there exists a small time interval when both phases are excited the mutual torque produced out of it will be very small.

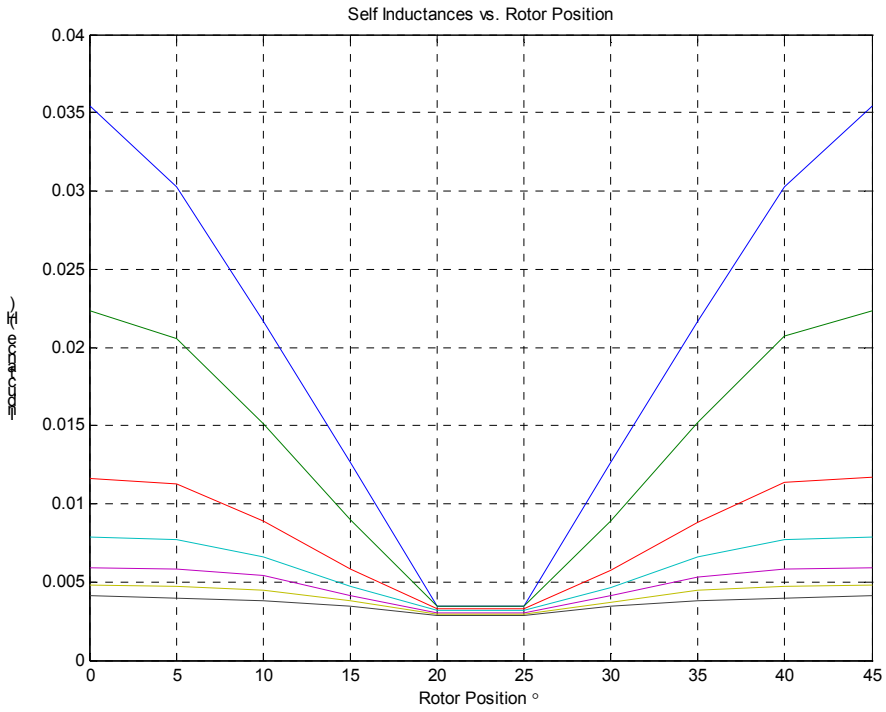

Figure 4.19 : Self Inductances (Laa) vs. Rotor Position for currents 0-90 A

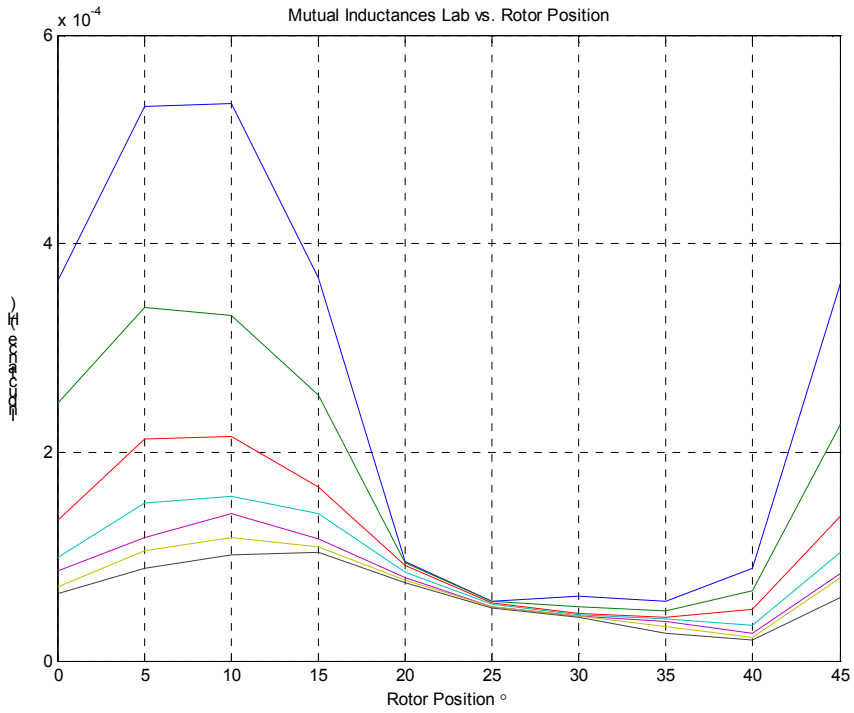

Figure 4.20 : Mutual Inductances vs. Rotor Position (Lab) for currents 0-90A

Torque generated is the most important result of all. After all, that is the main concern of this material. Figure 4.21 gives the results of the simulation for this concern.

It says that, at 45A it is possible get torque value of 35N, and at 90A it's able to supply a torque of 70Nm. It's also clear that for two positions, aligned and unaligned, torque production is 0 Nm.

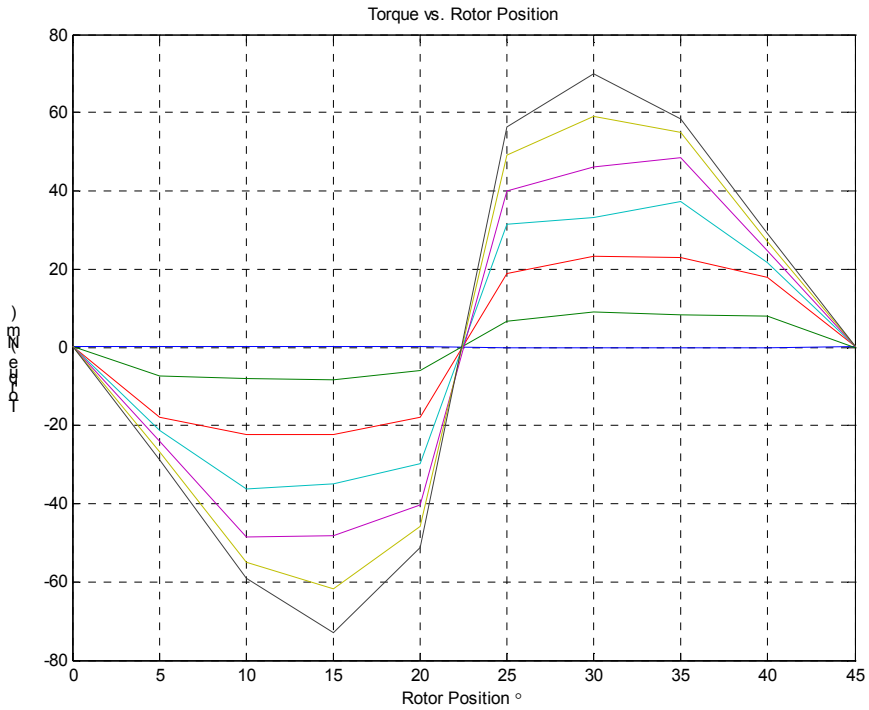

Figure 4.21 : Torque vs. Rotor Position for currents 0-90 A

The general appearance of the graph may look quite like what the theory says. However, there is one thing that may not be comforting; there is no constant torque region at all. Actually, anyone who looks at the inductance profiles can tell this is expected. Inductances are ever-changing, there is no constant region. This means partial derivative of the inductance with respect to rotor position is never zero. Therefore, it is reasonable in that sense. The point is this unwanted because it will increase the torque ripple. However, in this case since the machine will be mounted to vehicle of 1250 kg, and the equivalent inertia of this mass most probably will render this ripple insignificant in the end.

It is possible to see the continuous torque production in Figure 4.22. Continuous torque production is achieved by exciting all three phases with a phase difference. That phase difference is given by ε the stroke angle. In this case it is 15°.

That magic moment, when one phase is shut down and the next one must be turned on, can be measured from the graph. It's around 22°

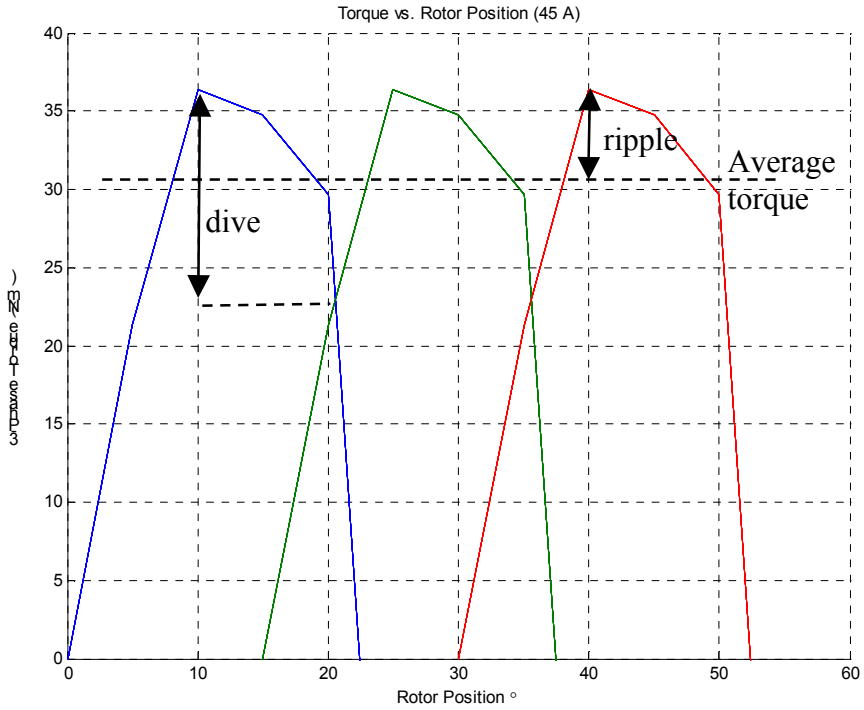

Figure 4.22 : Continuous torque production (45 A)

Another output of this simulation is the Torque-Current-Angle surface. (Figure 4.23) This surface shows the torque as a function of current, and rotor position. Cutting this surface with various torque planes gives the Torque Contour graph.(Figure 4.24) These two data can be valuable in order to see the capabilities of the motor. For instance, looking at the Torque-Contours, it can be clearly seen that around 5° only it is necessary to climb to a current level of 90A, or before 5° it is almost impossible to get a torque of 50 Nm. Moreover, this data is used in offline schemes that are used to control SRM. [1]

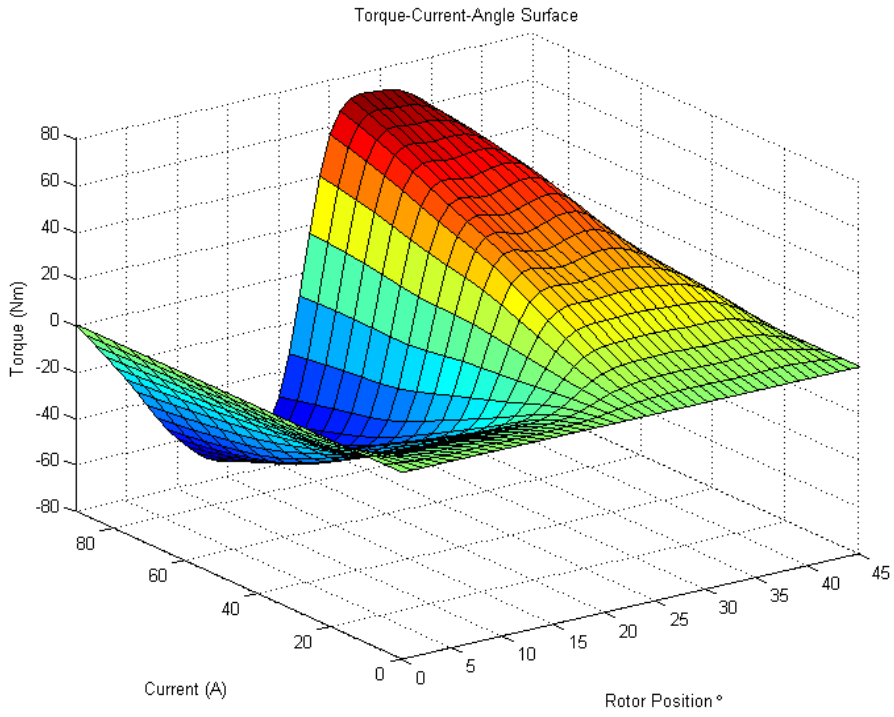

Figure 4.23 : Torque-Current-Rotor Position surface

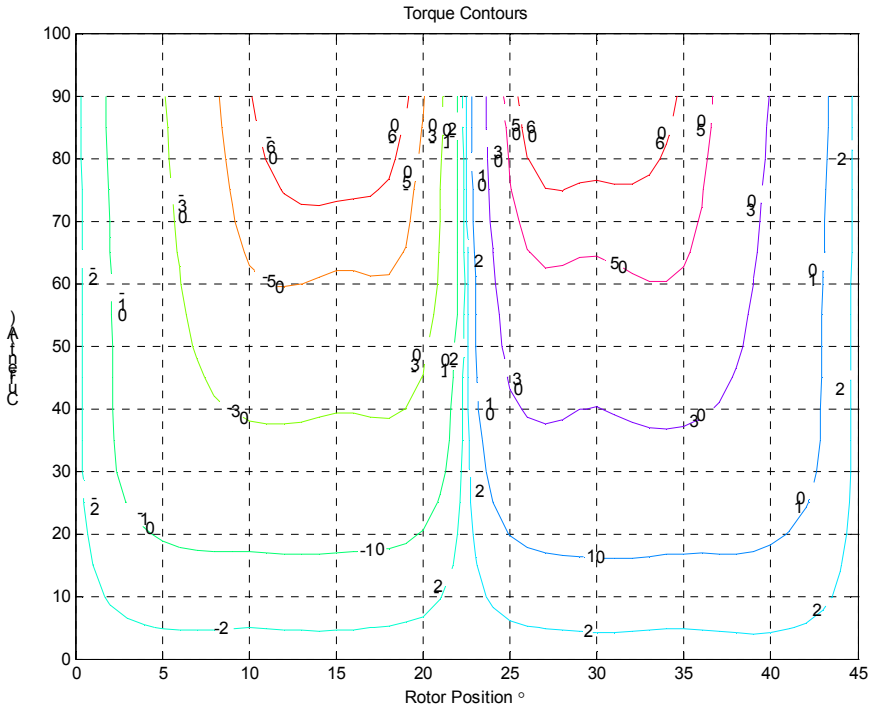

Figure 4.24 : Torque contours for various torque values

4.2.3 Simulink Model

Simulation results of the previous section shows many useful information. However, they are the product of Maxwell2D magnetostatic solver. Generally it is required to know transient behavior of the motor, so that one can observe the current, derivative of the current, back-emf, and voltage profiles during the operation.

A simulink model was prepared for this purpose.(Figure 4.30) The main idea behind this sort of 'unique '. System does not use a full analytical solution, but instead it uses the benefits of the FEA solution that has been created by the Maxwell magnetostatic solver. It utilizes look-up tables to embed those data in to the system and the rest is built on the equivalent electric circuit model of SRM. In a way, it can be called a hybrid model.

First monomer necessary to build the block model was a module that would give the inductances for given rotor position, and the phase currents. A 4-D look-up table was used for this. The block uses the 4 dimensional data from matlab workspace which was imported from Maxwell2D parametric solution table.

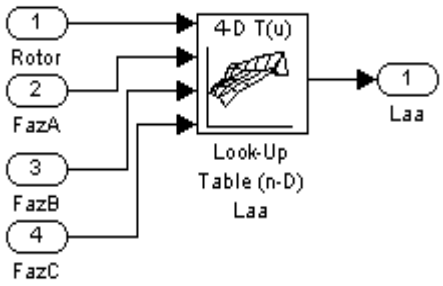

Figure 4.25: 4D Look-up table structure for inductance used in simulink

If the equation 2.xxx is unfolded, it will look like this;

$$V_{DC} = \left(\begin{bmatrix} R_a & 0 & 0 \\ 0 & R_b & 0 \\ 0 & 0 & R_c \end{bmatrix} + \frac{d}{dt} \begin{bmatrix} L_{aa} & L_{ab} & L_{ac} \\ L_{ba} & L_{bb} & L_{bc} \\ L_{ca} & L_{cb} & L_{cc} \end{bmatrix} \right) \begin{bmatrix} i_a \\ i_b \\ i_c \end{bmatrix} + \begin{bmatrix} L_{aa} & L_{ab} & L_{ac} \\ L_{ba} & L_{bb} & L_{bc} \\ L_{ca} & L_{cb} & L_{cc} \end{bmatrix} \frac{d}{dt} \begin{bmatrix} i_a \\ i_b \\ i_c \end{bmatrix} \quad (4.33)$$

Therefore, those inductance matrixes have to be constructed by using the inductance monomer. Figure 4.26 shows the way to do this. One thing to keep in mind is that, Maxwell2D gives the inductance results per meter and uses Amper-Turn values in FEA.

Inducta of
the mot

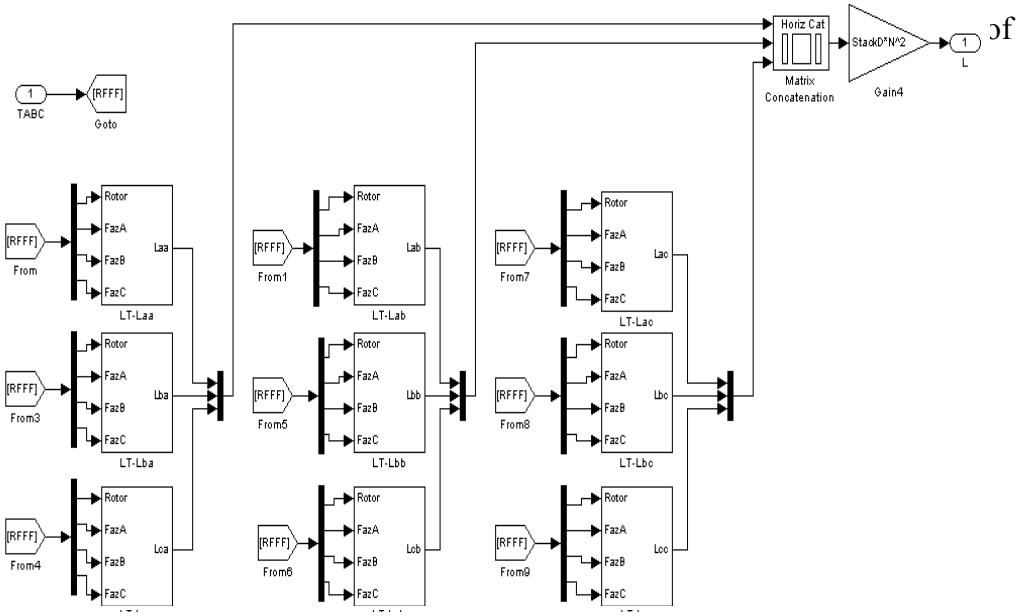

Figure 4.26 : Inductance matrix structure used in simulink

Torque can be read the same way the inductance is read. (See Figure 4.27)

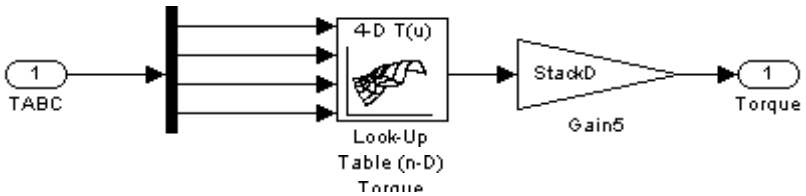

Figure 4.27 : 4D Look-up Table Structure used in Simulink for Torque

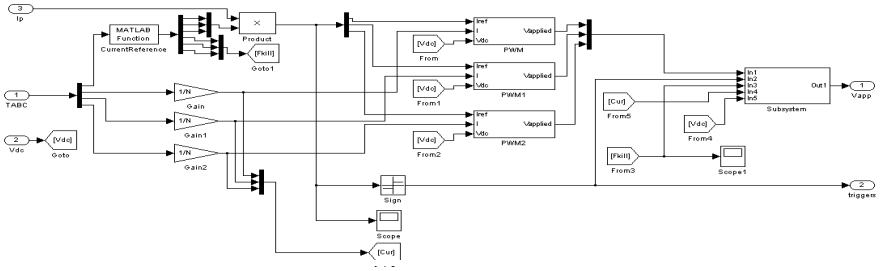

Figure 4.28 : Block Structure Used to Simulate Switching

Working principles of asymmetric half bridge was explained before in this chapter. When the switches of the phase opens, current drops to zero, and the diodes do not let it become negative. This can be achieved by using a saturation block in the

simulink. However, since this current is integrated from di, that can not be driven to zero as it happens in real life. Therefore, the effects of this unwanted derivative of the current have to be canceled out. The compensation module for this can be seen below in Figure 4.29

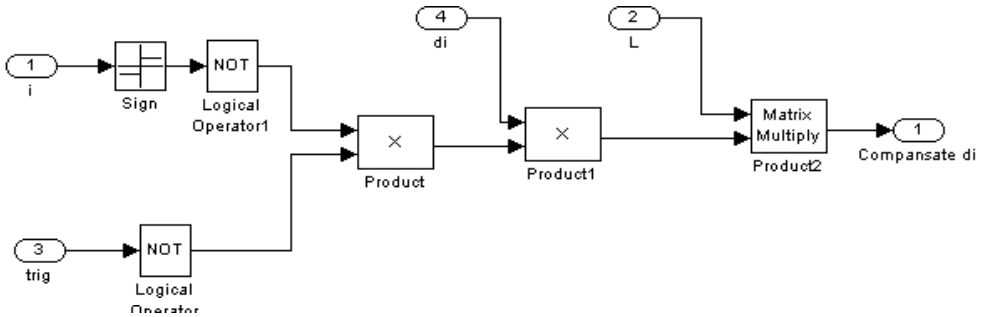

Figure 4.29 : Block structure for AH -bridge diode characteristics compensation

Entire system looks like as follows;

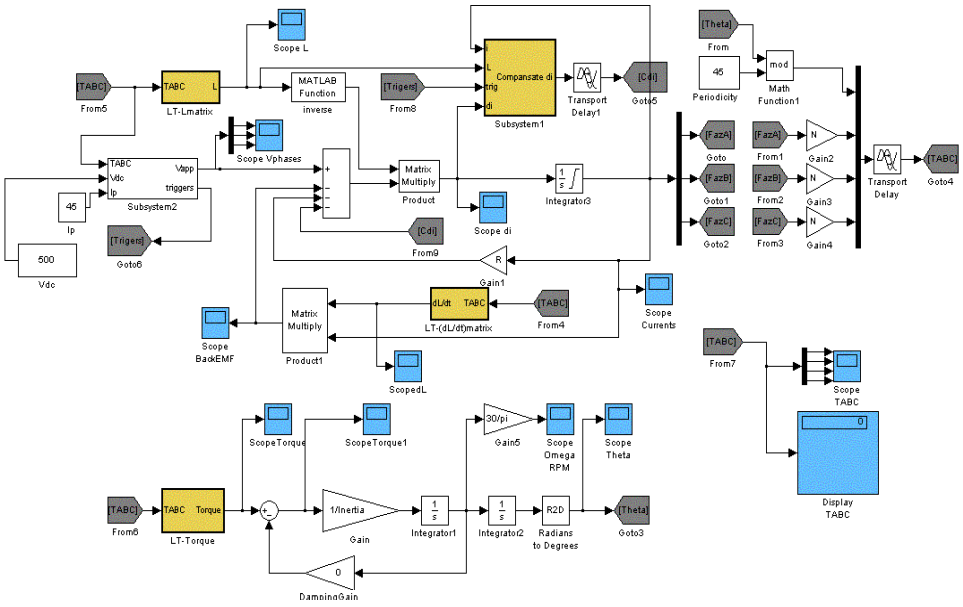

Figure 4.30: Simulink block diagram of full system

Doing the simulations with a current controller driving a current 45A in trapezoidal profile the following results are obtained:

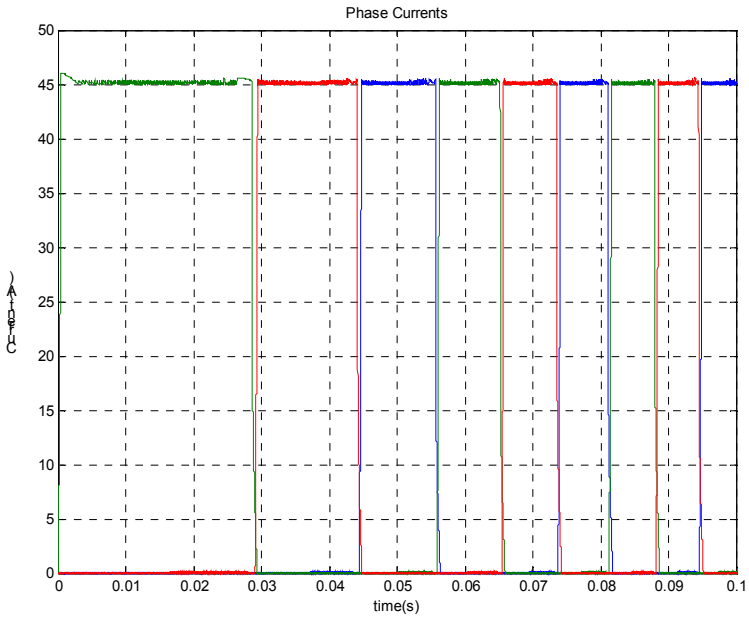

Figure 4.31 : Controlled phase currents

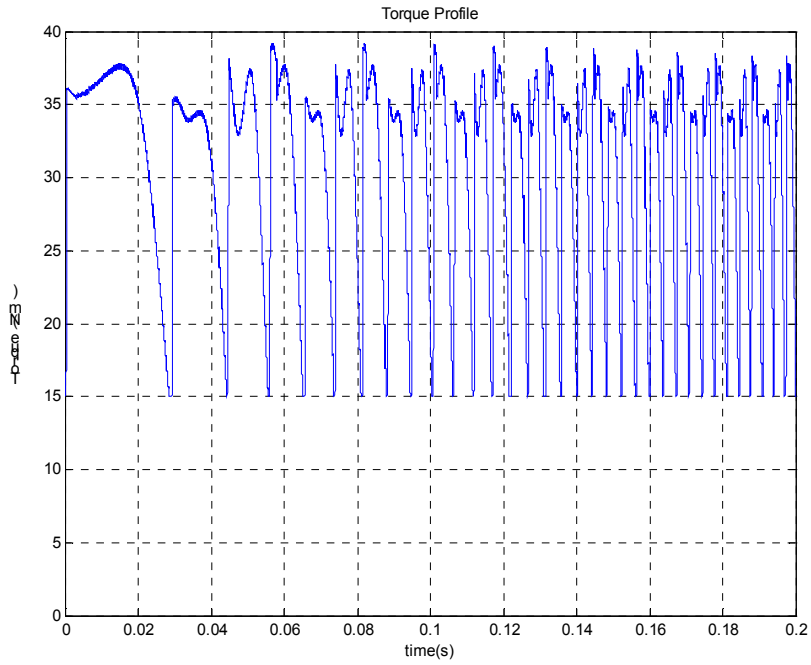

Figure 4.32 : Torque Profile

Torque results reveal the amount of ripple. It is more than 50%. However the maximum torque is around 35Nm and the average can be found as 32 Nm. These are coherent with the Maxwell results. The effect of ripple on the vehicles velocity can be

seen inFigure 4.36. It has actually no effect because of the high equivalent inertia of the car.

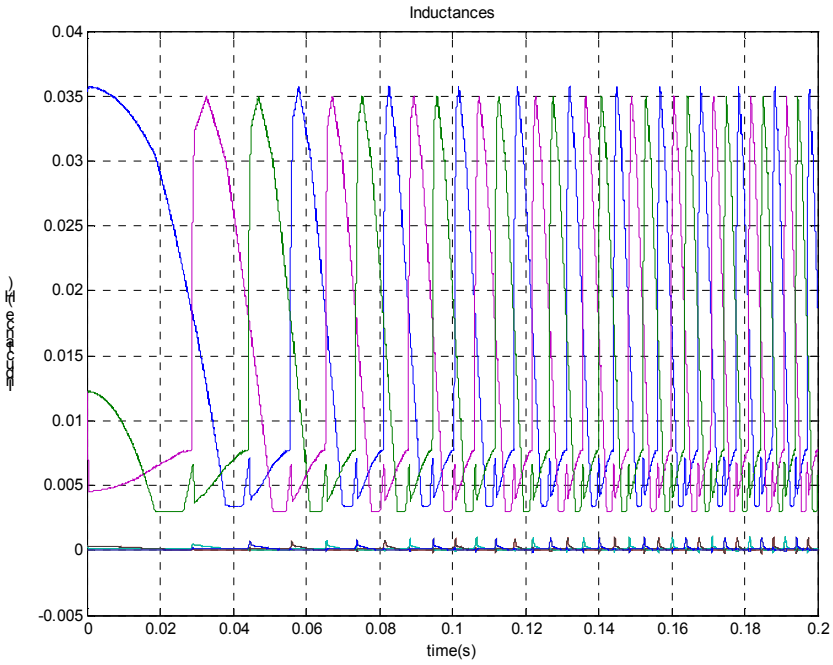

Figure 4.33 : Inductance Profiles (Self & Mutual)

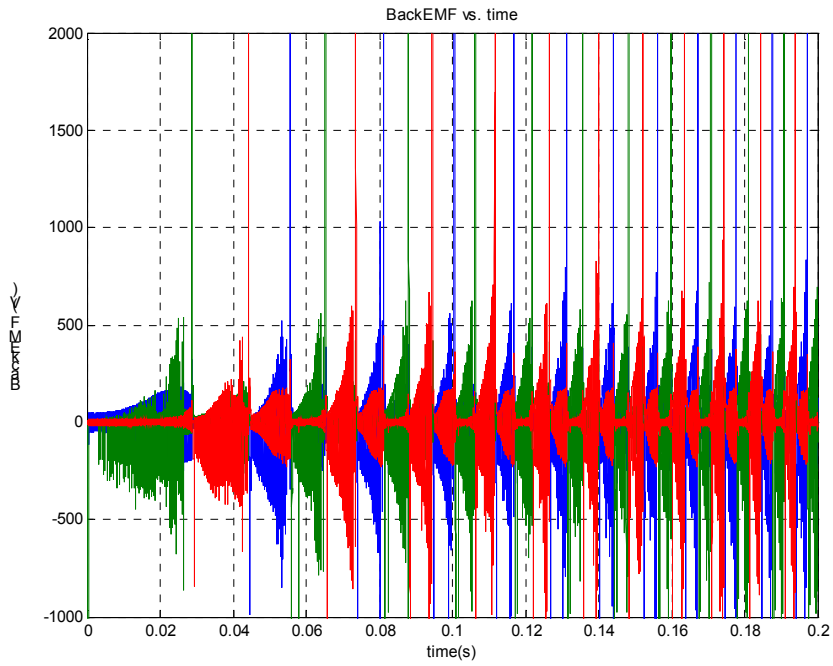

Figure 4.34 : Back EMF

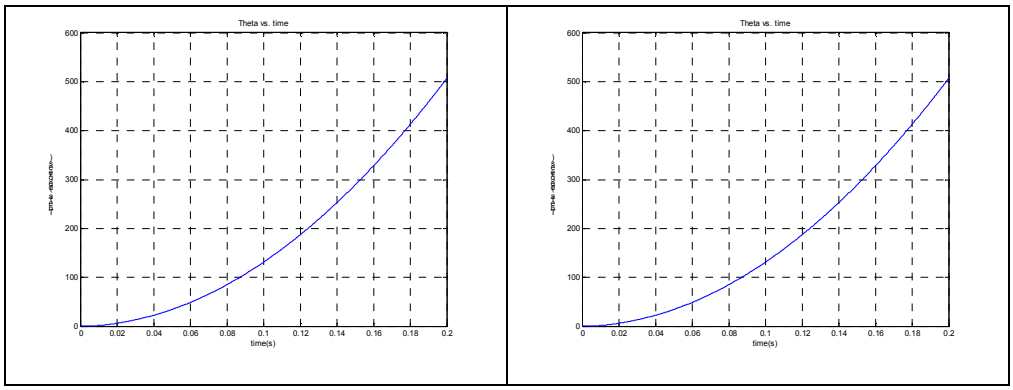

Figure 4.35 a) Theta in degrees b)Omega in rpm

Moreover, vehicles model can be embedded into this simulation in order to get some idea about the performance. Below performance speeding performance of a 1250 vehicle can be found. The torque reference for this test has be shaped so that for first 30 seconds the current will be tripled and after the phase is over it will drop the double for 10 seconds and in the end it will reach the base current.

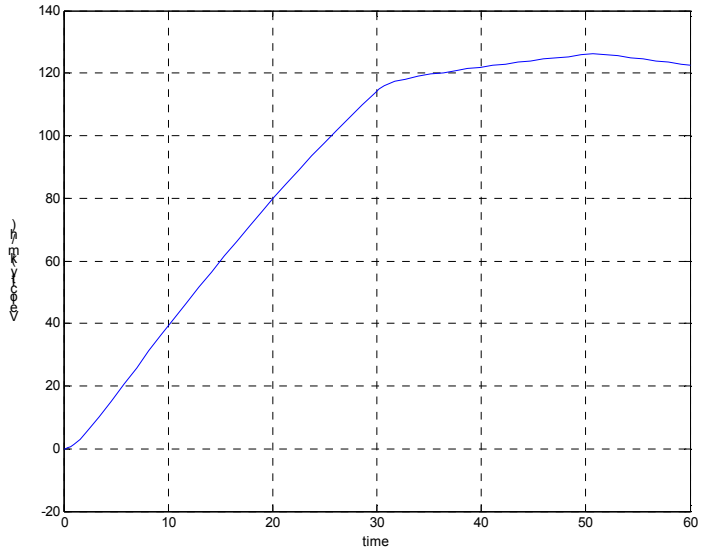

Figure 4.36 : Speeding curve of a hypothetical vehicle

4.3 Inverter-Driver Proposal

There are many different inverter topologies that are being used for SRM. Some of them are; Asymmetrical Half Bridge Inverter, Miller Inverter, Six Switch Converter,

Buck Converter, Split Capacitor Converter. All the topologies have different advantages and disadvantages, but the most utilized scheme is Asymmetric Half Bridge structure.

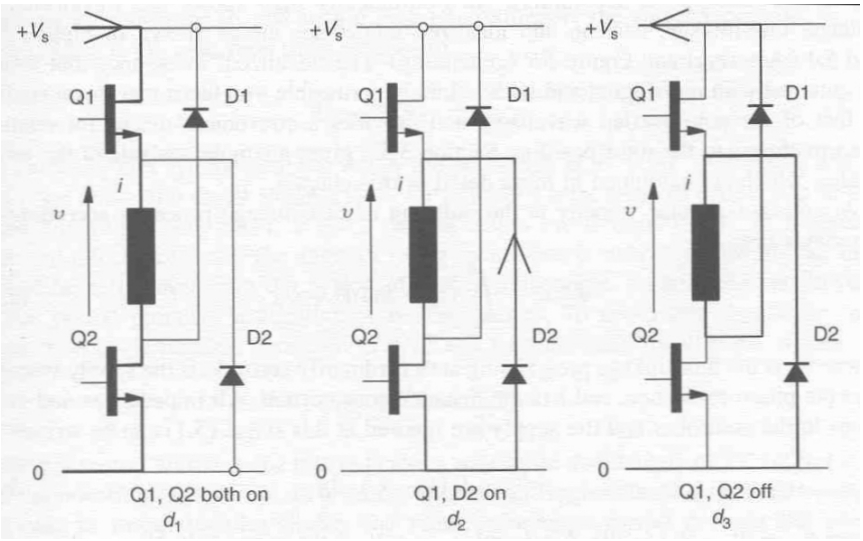

Figure 4.37 : Asymetric Half Bridge Inverster

Even though it can not be argued that it uses the minimum number of power switches (which may be important to feasibility), it certainly capable of many actions may be needed to drive the machine. It can energize and de-energize the winding for sure. It permits soft switching, so a zero voltage free wheeling state can be obtained.

For this project, this structure has been selected. As for the half bridge modules, SKF 300 GAR 123D and SKF 300 GAL 123 D are chosen.

4.4 Heat Transfer

Through out the iterative process explained in dimensioning section, it turned out that the maximum current that can flow through the windings is the Achilles' heel for this struggle. High value of A_s gives higher torque, but then requires high i or T_{ph} for this. To be able to fit a high number of turns for the winding, the diameter of the coil wire (magnet-wire) must be small. Then the ampacity (current capacity) drops down. It needs a careful examination, but the main idea is to be able to push the ampacity as much as possible.

No detailed heat transfer analysis has been applied for the design. Instead, standard rules of National Electric Code (NEC 2001 of NEMA (National Electrical Manufacturers Association)) were followed. These standards are compiled for every

possible branch of electric engineering and contain a chapter on motor winding regulations also. Their focus is to guarantee the safety, durability and the reliability of electrical systems.

A software, WireTronic, was used to get necessary information on the magnet-wire that will be used in phase windings. This program gives the diameter, isolation coating thicknesses, and the current capacity (ampacity) of the magnet-wire.

It may be a good idea to give some information about the magnet-wire also. The term "magnet-wire" is used to describe solid conductor wire (usually copper), insulated with a polymer based film. The films are designed to provide a uniform dielectric coating while taking up as little space as possible. There are a variety of film insulations available for magnet wire offering different characteristics. The primary classification factor for magnet wire is "Thermal Class." Thermal class is the recommended maximum continuous operating temperature for the insulation. Standard thermal classes range from 105 degrees Celsius up to 220 degrees Celsius. The Institute of Electrical and Electronics Engineers (IEEE) define thermal classes of insulation by upper temperature limits at which the untreated insulation will have a life expectancy of at least 20,000 hours.

Table 4.1 : Thermal Classes

Thermal Isolation Class	Temperature Limit (°C)	Insulation Coatings
O	80	cotton, paper, silk
A	105	oleoresinous and formvar enamels, varnish-treated cotton, polyurethane
B	130	polyurethanes, polyurethane-nylons
F	155	Polyurethane-155
H	180	asbestos, mica, silicone varnishes, and polyamide, Teflon

Source: "McGraw-Hill Encyclopedia of Science & Technology", Vol. 10 LEP-MES, 8th Edition, (c) 1997, ISBN 9-07-911504-7 (set

The basic ambient temperature rating point of most motors is 40°C. A motor rated for 40°C is suitable for installation where the normal surrounding air temperature does not exceed 40°C (104°F). This is the starting point. When the motor operates at full load, it has a certain temperature rise, which adds to the ambient temperature. For

example, U frame motors originally had Class A insulation and a maximum temperature rise of 55°C. In a 40°C ambient temperature, this gives an average winding temperature of 95°C. That's 40°C (ambient) plus 55°C (rise). Manufacturers use the 10° difference between 95°C and 105°C rating of Class A insulation to handle the hot spot allowance.

Motors generally use these components for insulation;

- Enamel coating on the magnet wire.
- Insulation that comes to the conduit box.
- Sleeving where leads connect to magnet wire.
- Lacing string that binds the end turns of the motor.
- Slot liners (in the stator laminations) that protect the wire from chafing.
- Top sticks that hold the wire down in place inside the stator slots.
- Varnish that manufacturers dip the completed assembly in, prior to baking it. The dipping varnish seals nicks or scratches that may occur during the winding process. The varnish also binds the entire winding together into a solid mass so it doesn't vibrate and chafe when subjected to the high magnetic forces.

Since 45A is the rated current for this design, suitable conductor size must be selected for that current value. Ampacity tables generally give the current capacity of a single wire at a specific temperature. However, when the there is a bundle or a group of wires closely placed, that values decreases. Same applies for the temperature also. Ampacity table data are generally for ambient temperature of 20-35 C. If any of these conditions above is different in the particular design correction factors have to be used.

Those corrections factors are called derateing coefficients. In this design derating will be necessary only for the number of conductors. In the winding of a stator phase there will be 120 wires closely packed inside the motor. Their current capacity will be certainly lower than that of a single wire. Derating coefficient for a bundle increases with the number of wires in the bundle, but as the number of wires exceeds 25 the coefficient converges to a value of 0.45. In this design, it means that if a current of 45A is the target, a magnet wire capable of carrying 100A will do just fine. As for the temperature, there is no need for derating, since the ambient temperature for the designed motor will be more or less between 25 - 40 C, which are almost the values the NEC data are derived for.

Before jumping into the wire ampacities, there is one more thing to consider. This machine is a three phase machine, but never any of the two windings are excited at the

same time. According to the rotor position the phases are ignited one by one successively. This means that wires are not conducting with a 100% duty ratio. In fact, their duty ratio is %33,3 for a changing period of motoring cycle. This should somewhat relief the constrains on the ampacity. If not the duty ratio is used to re-rate the wire ampacity, at least RMS current can be used. RMS current for this 6/8 SRM is;

$$I_{rms} = \frac{I_p}{\sqrt{q}} = \frac{I_p}{\sqrt{3}} \tag{4.34}$$

As a result, a magnet-wire capable of carrying $\frac{100}{\sqrt{3}} \cong 60A$ is what is needed for the design.

Wiretron can give the ampacity for a selected wire, along with its dimensions like diameter, insulation thickness, and its resistance value as Ω/m. Using the software magnet-wire of 9AWG has chosen for the motor. Some dimensions and properties can be seen in the table below.

Table 4.2 : Chosen Magnet-wire Properties

Property	**Value**	**Unit**
Wire size	9	AWG
Diameter (nominal)	2.9058	mm
Resistance	0.002598	Ω/m
Insulation type	Heavy	--
Insulated diameter	2.9896	mm
Ampacity (40°C)	62.5	A

This current limit is for safe use under continuous working conditions. However, it does not mean that this value can never be exploited. For short periods of time current driven can be doubled or tripled. Moreover, if any active cooling exist, motor can definitely be promoted to a higher power rank.

5 CONCLUSION & DISCUSSION

In this work an experimental in-wheel motor prototype has been designed. The necessity emerged from a plan to work on electric vehicle's control with 4-wheel independent drive configuration. Since it is much easier to use an already existing infrastructure, the proposed design had to be compatible with the class A cars on the market. The final product perfectly fits into a standard R14 wheel, and can be easily mounted to the knuckle of every class C car on the roads today. In addition the prototype will be able withstand the forces that were foreseen during the design. This means that with a proper control scheme, everything is ready to test it on the road.

The prototype's power can be argued to be its minus. Results of the simulink simulation show that it accelerates slower than a mediocre commercial IC engine vehicle. However, that performance criteria was never part of the design. Even it was, it might not be solved, at least with this configuration of SRM. A careful eye would catch it; the torque production zone, the laminations' stack thickness id only a 33% of the available space inside the wheel. In order to boost the design into a more dexterous machine, that problem has to be solved.

During the experimentation many aspects which were deliberately ignored in this thesis can be observed and considered as a data for the next design iteration. These are: acoustic noise level of the motor, effect of variation of air-gap thickness due to forces acting on the tyre and performance change of motor due to heat dissipation issues.

In the end, motor was designed and the simulations tell that the design specifications and the outputs are coherent and comparable. By the time this thesis is being written, the parts of the motor are being produced and will be ready for experimenting in a week.

Under these circumstances it can be counted as a successful and fruitful project.

REFERENCES

[1] "Milestones", http://www.wavecrestlabs.com

[2] Baker, David, Lunar Roving Vehicle: Design Report, *Spaceflight,* 13, 234-240, July 1971

[3] Stone, H. W., **Design and Control of the MESUR/Pathfinder Microrover**, *Proceedings of the 1993 International Conference on Advanced Robotics*, Tokyo, Japan, November 1993. PostScript version

[4] Fitzgerald. A.E., Jr. Kingsley. C, Umans. S. D., "Electric Machinery", Mc Graw Hill, 1992

[5] Krishnan. R., "Switched Reluctance Motor Drives", CRC Press, 2001

[6] Anderson. F.A., "Development History", *Electronic Control of Switched Reluctance Machines*, Newnes Power Engineering Series, 2001

[7] Miller. T.J.E., "Electronic Control of Switched reluctance machines", Newnes Power Engineering Series, 2001

[8] Radun, A.V., "Design considerations for switched reluctance motor", *IEEE Trans. On Industry Appl*., 31, 1049-1087, 1995

[9] Miller, T.J.E. and M. McGilp, "Nonlinear theory of the switched reluctance motor for computer-aided design", *IEEE Proc. B*, 137(6),337-346,1990

[10] Evers, W., Reichel, J., Eisenkolb, R., Enhart, I., "The wheel dynamometer as a tool for chassis development", Kistler Instrumente AG, SD920-234e,2002

[11] Amman, M., Evers, W., Streilein, V., "RoaDyn™-a development Tool for Braking Systems", Kistler Instrumente AG, SD920-234e,2002

[12] Arumugam, R., J.F. Lindsay, and R. Krishnan, "Sensitivity pole arc/pole pitch ratio on switched reluctance motor performance", IEEE Ind. Appl. Soc. Ann. Mtg. Conf. Rec., Oct. 1988, Pitsburg, PA, pp. 50-54

6 APPENDIX

6.1 3D Model of the Motor

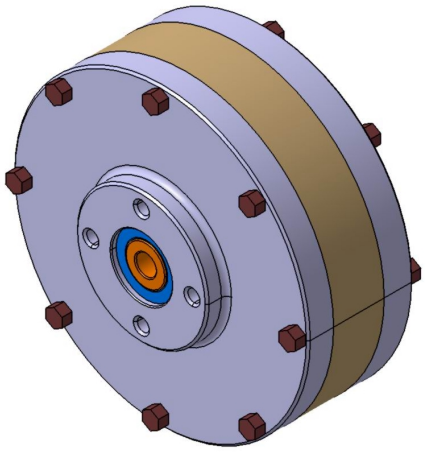

Figure 6.1 : Isometric View of Motor (Front)

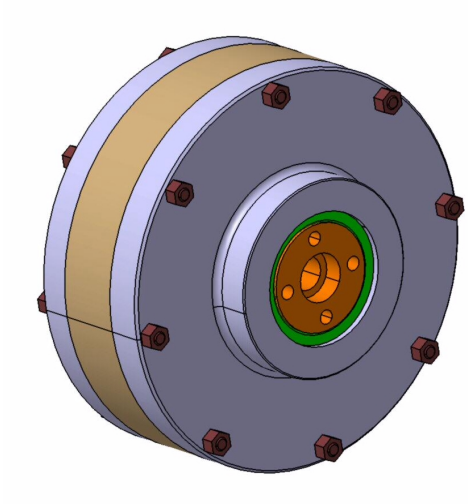

Figure 6.2 : Isometric View of Motor (Rear)

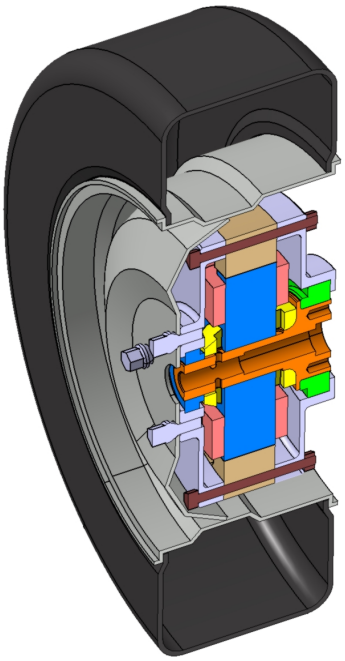

Figure 6.3 : 3D Cutaway cross-section of full system

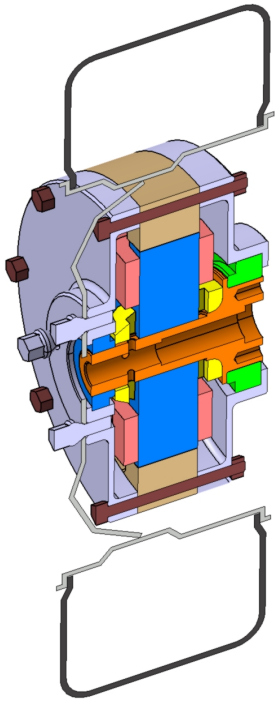

Figure 6.4 : 'Motor only' 3D cross-sectional view

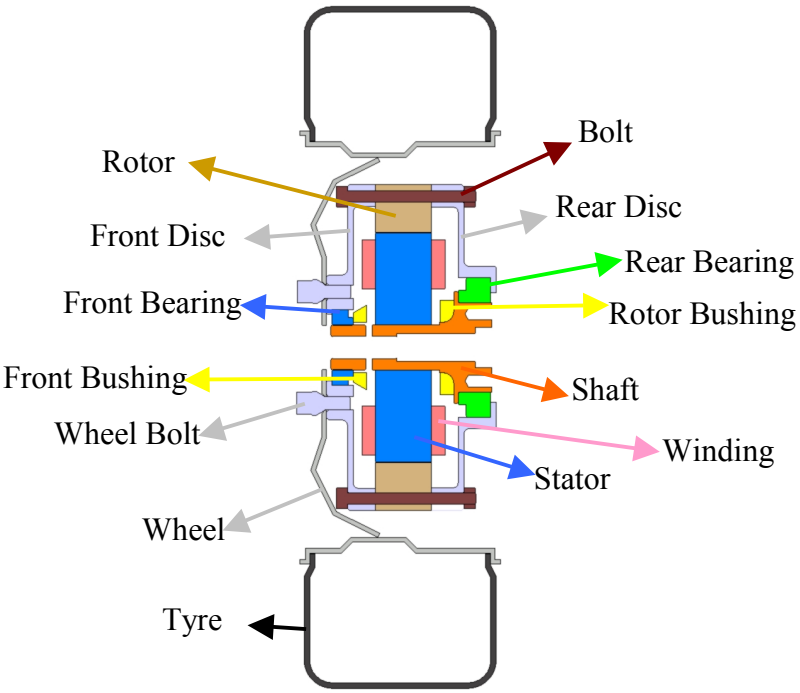

Figure 6.5 : Detailed cross-section

6.2 SPECIFICATIONS OF THE MOTOR

Table 6.1 : Motor's specifications

Number of Stator Poles	6
Number of Rotor Poles	8
Stator Pole arc β_s	18°
Rotor Pole arc β_r	22°
Air-gap thickness l_g	0.4 mm
Stack length L	50 mm
Bore diameter D	200 mm
Shaft diameter D_s	45 mm
Rotor outer diameter	290 mm
Back-iron thickness	22mm
Turn/phase	120
Coil wire dimension	9 AWG
Base current	45 A
Lamination material	M19 steel
Phase resistance	0.06 Ω
Copper Loss (@base current)	120 W
Average torque (900 rpm)	33 Nm
Continuous Power	3.2kW
Peak Power	9 kW
Insulation Class	B

6.3 B-H CURVE

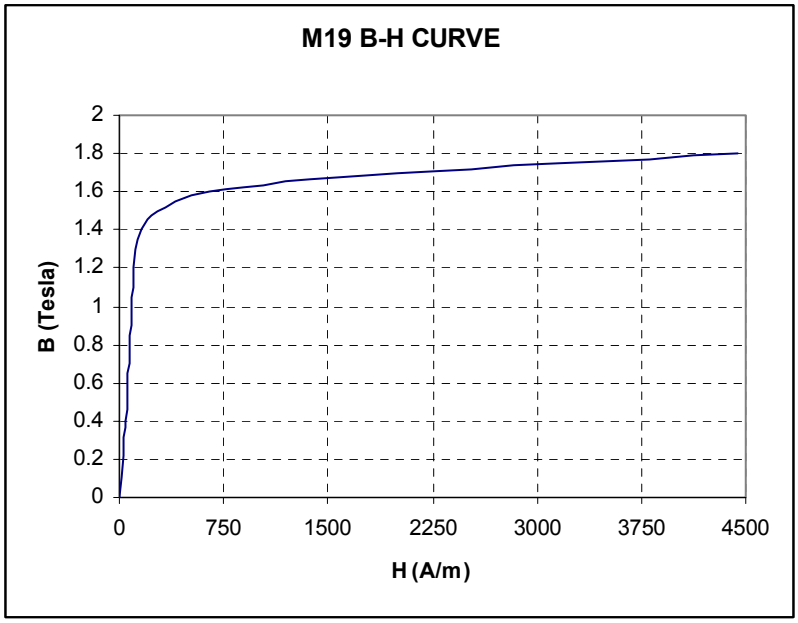
M19 B-H CURVE
B (Tesla)
2
1.8
1.6
1.4
1.2
1
0.8
0.6
0.4
0.2
0
0
750
1500
2250
3000
3750
4500
H (A/m)

REFERENCES

[1] "Milestones", http://www.wavecrestlabs.com

[2] Baker, David, Lunar Roving Vehicle: Design Report, *Spaceflight,* 13, 234-240, July 1971

[3] Stone, H. W., **Design and Control of the MESUR/Pathfinder Microrover**, *Proceedings of the 1993 International Conference on Advanced Robotics*, Tokyo, Japan, November 1993. PostScript version

[4] Fitzgerald. A.E., Jr. Kingsley. C, Umans. S. D., "Electric Machinery", Mc Graw Hill, 1992

[5] Krishnan. R., "Switched Reluctance Motor Drives", CRC Press, 2001

[6] Anderson. F.A., "Development History", *Electronic Control of Switched Reluctance Machines*, Newnes Power Engineering Series, 2001

[7] Miller. T.J.E., "Electronic Control of Switched reluctance machines", Newnes Power Engineering Series, 2001

[8] Radun, A.V., "Design considerations for switched reluctance motor", *IEEE Trans. On Industry Appl*., 31, 1049-1087, 1995

[9] Miller, T.J.E. and M. McGilp, "Nonlinear theory of the switched reluctance motor for computer-aided design", *IEEE Proc. B*, 137(6),337-346,1990

[10] Evers, W., Reichel, J., Eisenkolb, R., Enhart, I., "The wheel dynamometer as a tool for chassis development", Kistler Instrumente AG, SD920-234e,2002

[11] Amman, M., Evers, W., Streilein, V., "RoaDyn™-a development Tool for Braking Systems", Kistler Instrumente AG, SD920-234e,2002

[12] Arumugam, R., J.F. Lindsay, and R. Krishnan, "Sensitivity pole arc/pole pitch ratio on switched reluctance motor performance", IEEE Ind. Appl. Soc. Ann. Mtg. Conf. Rec., Oct. 1988, Pitsburg, PA, pp. 50-54